JPn Neuroscience

The Journal of Physiology

J Physiol 594.10 (2016) pp 2729–2749

Time-invariant feed-forward inhibition of Purkinje cells in the cerebellar cortex *in vivo*

Antonin Blot[1,*], Camille de Solages[1,*], Srdjan Ostojic[2], German Szapiro[1], Vincent Hakim[3,4,5] and Clément Léna[1]

[1] *IBENS, École Normale Supérieure, PSL Research University, CNRS, INSERM, Paris, France*
[2] *Laboratoire de Neurosciences Cognitives, École Normale Supérieure, PSL Research University, CNRS, INSERM, Paris, France*
[3] *Laboratoire de Physique Statistique, École Normale Supérieure, PSL Research University, CNRS, Paris, France*
[4] *Sorbonne Universités, UPMC Université, Paris, France*
[5] *Sorbonne Paris Cité, Université Paris Diderot, Paris, France*

Key points

- We performed extracellular recording of pairs of interneuron–Purkinje cells *in vivo*.
- A single interneuron produces a substantial, short-lasting, inhibition of Purkinje cells.
- Feed-forward inhibition is associated with characteristic asymmetric cross-correlograms.
- *In vivo*, Purkinje cell spikes only depend on the most recent synaptic activity.

Abstract Cerebellar molecular layer interneurons are considered to control the firing rate and spike timing of Purkinje cells. However, interactions between these cell types are largely unexplored *in vivo*. Using tetrodes, we performed simultaneous extracellular recordings of neighbouring Purkinje cells and molecular layer interneurons, presumably basket cells, in adult rats *in vivo*. The high levels of afferent synaptic activity encountered *in vivo* yield irregular spiking and reveal discharge patterns characteristic of feed-forward inhibition, thus suggesting an overlap of the afferent excitatory inputs between Purkinje cells and basket cells. Under conditions of intense background synaptic inputs, interneuron spikes exert a short-lasting inhibitory effect, delaying the following Purkinje cell spike by an amount remarkably independent of the Purkinje cell firing cycle. This effect can be explained by the short memory time of the Purkinje cell potential as a result of the intense incoming synaptic activity. Finally, we found little evidence for any involvement of the interneurons that we recorded with the cerebellar high-frequency oscillations promoting Purkinje cell synchrony. The rapid interactions between interneurons and Purkinje cells might be of particular importance in fine motor control because the inhibitory action of interneurons on Purkinje cells leads to deep cerebellar nuclear disinhibition and hence increased cerebellar output.

(Received 3 September 2015; accepted after revision 15 February 2016; first published online 26 February 2016)
Corresponding author C. Léna: 46 rue d'Ulm, Paris 75005, France. Email: lena@biologie.ens.fr

Abbreviations DSC, delayed-spike curve; ISI, interspike interval; LFP, local field potential; PC, Purkinje cell; STA, spike-triggered average.

Introduction

In the central nervous system, the level of activity and its organization are considered to be conditioned by inhibition (Pouille & Scanziani, 2001; Brunel *et al.* 2004; Mittmann *et al.* 2005). Inhibitory interneurons also participate in the generation of oscillations of various frequencies (Csicsvari *et al.* 1999; Klausberger & Somogyi, 2008), and modulate dendritic integration (Rudolph *et al.* 2007; Rothman *et al.* 2009) and synaptic plasticity (Jörntell & Ekerot, 2003; Lamsa *et al.* 2005). How interneurons carry out these functions remains poorly understood, notably

*These authors contributed equally to this work.

DOI: 10.1113/JP271518

because of their phenotypic heterogeneity (Ascoli *et al.* 2008; DeFelipe *et al.* 2013). The simultaneous recording of principal cells and defined local interneurons is therefore often very difficult.

In the cerebellum, principal neurons (i.e. the Purkinje cells) are contacted by two types of interneurons situated in the molecular layer: the stellate cells and the basket cells. Molecular layer interneurons presumably mediate both feed-forward and lateral inhibition (Andersen *et al.* 1964; Eccles *et al.* 1967; Cohen & Yarom, 2000; Brunel *et al.* 2004; Mittmann *et al.* 2005; Dizon & Khodakhah, 2011; Park *et al.* 2012). *In vitro*, they strongly regulate the firing of spontaneously active Purkinje cells (Häusser & Clark, 1997). These interneurons are considered to be essential for motor learning (Wulff *et al.* 2009) and may promote movements by inhibiting Purkinje cells and thus disinhibiting the cerebellar nuclei (Heiney *et al.* 2014).

Purkinje cells are GABAergic neurons that form the sole output of the cerebellar cortex. They mediate the tonic inhibition of deep cerebellar nuclear principal cells on which they converge (de Zeeuw & Berrebi, 1995) and activate inhibitory currents with a decay time <3 ms (Person & Raman, 2011). A precise organization of the Purkinje cell population activity is therefore needed to relieve this inhibition (Isope *et al.* 2002; Person & Raman, 2012). Purkinje cells also project to other Purkinje cells (and possibly to molecular layer interneurons) (Palay & Chan-Palay, 1974; Orduz & Llano, 2007; Watt *et al.* 2009) and thus form a recurrent inhibitory network. Such a network with rapid somatic inhibitory currents, as found in adult Purkinje cells (de Solages *et al.* 2008), may generate very fast oscillations; indeed, we have shown previously that Purkinje cell activity *in vivo* is organized in high-frequency ($\sim$200 Hz) population oscillations (de Solages *et al.* 2008). Whether molecular layer interneurons contribute to this activity is not known, mainly because the interactions between interneurons and Purkinje cells *in vivo* remain largely unexplored (Bengtsson *et al.* 2013).

In the present study, using simultaneous recordings of basket and Purkinje cells with tetrodes in adult anaesthetized rats, we show that interneurons mediate feed-forward inhibition *in vivo* (Andersen *et al.* 1964; Eccles *et al.* 1967), an idea that had been brought into question previously (Ekerot & Jörntell, 2001; Jörntell & Ekerot, 2002; Jörntell *et al.* 2010). Purkinje cell and molecular layer interneuron activities are co-modulated, although the latter do not appear to participate in the 200 Hz oscillations. Interneuron synchrony strengthens but does not prolong the inhibition of Purkinje cell firing. We demonstrate that this inhibition is independent of the firing history of Purkinje cells, although only in the presence of high levels of afferent activity. These results reveal a complex organization of the molecular layer comprising two interconnected cell types with differing population organization, and indicate that the integrative properties of Purkinje cells are strongly modified by high levels of ongoing activity, such as those encountered *in vivo*.

Methods

Animals

The experimental procedures were conducted in conformity with the institutional guidelines and in compliance with national and European laws and policies. Experiments were performed on male adult Wistar Han rats (3–5 months old; 400–600 g; Charles River Laboratories, Saint-Germain-Nuelles, France).

In vivo electrophysiology

After the induction of anaesthesia with a ketamine–xylazine mixture (100 and 10 mg kg^{-1}, respectively, in saline), the animal was mounted in a stereotaxic frame (David Kopf Instruments, Tujunga, CA, USA) and was maintained anaesthetized during the whole procedure with isoflurane (0.5–1.5% in O_2), for which the level was adjusted to keep the heart rate and blood oxygen concentration constant. A heating device controlled by rectal temperature was used to maintain the rat at physiological core temperature. Before incision of the scalp, 3% lidocaine was injected S.C. at the site of incision. The skull and dura over the vermian part of lobules V and VIa were removed using a dental drill, a curved syringe needle and fine forceps. Subdural meninges were gently removed where the electrodes were to be inserted. The surface of the cerebellum was kept moist with a saline solution. The present study also used data obtained in a chronically implanted rat with tetrodes using a home-made microdrive (Gao *et al.* 2012). The surgery for this animal was very similar, except for an injection of lidocaine (S.C.) before the incision, the addition of the microdrive, which was anchored to the skull using screws and dental cement, and the final suture of the wound before letting the animal wake up. The rat was left 2 days to recover before the beginning of tetrode adjustment.

Experiments and unit isolation were performed as described previously (de Solages *et al.* 2008; Gao *et al.* 2012). Extracellular potentials were acquired with a TDT system 3 (Tucker Davis Technologies, Alachua, FL, USA). Signals were referenced against a tungsten electrode positioned in saline at the surface of the cerebellar cortex. The signal from each channel was first filtered (0.1–8 kHz) with a Butterworth filter, then differentially amplified, sampled at 25 kHz and stored to disk for offline analysis. The activity was continuously monitored through loudspeakers and displayed on a computer screen.

Simultaneous multiple single unit recordings were obtained using tetrode recordings (Wilson & McNaughton, 1993; Delescluse & Pouzat, 2006). Multiunit activity was recorded from the Purkinje cell layer (as determined by the presence of complex spikes) either with hand-made 12 μm nickel-chrome wires (Goodfellow Cambridge Ltd, Huntington, UK) twisted together or commercial tetrodes (tungsten electrodes in a quartz matrix; Thomas Recording, Gießen, Germany) in the cerebellar vermis at depths ranging from 1 to 5 mm. Before recording, the tip of the wires were cleaned (Microelectrode Tip Cleaner; Thomas Recording) and gold-plated (gold solution; Sifco, Cleveland, OH, USA) to reduce their impedance to 200–300 kΩ. The tetrode was lowered vertically in small increments of 10–50 μm. The different layers of the cerebellar cortex could be discriminated during the experiments according to their specific features (Gao *et al.* 2012). In particular, the Purkinje cell layer was characterized by an intense cellular activity and distinctive complex spikes (Fig. 1*D*), which, in the proximal molecular layer, appeared as 1–3 ms broad monophasic negative waves.

Continuous recordings were first high-pass filtered at 300 Hz with a Butterworth filter before thresholding (typically at 50 μV). Single-unit spikes were isolated off-line by means of manual clustering ('xclust', M. A. Wilson, Massachusetts Institute of Technology, Cambridge, MA, USA) using the spike peak amplitudes. With these methods, three to seven units could be isolated per tetrode. The accuracy of unit isolation was assessed with two parameters: the fraction of spike counts in the $\pm$1 ms window of the autocorrelogram (P_{acorr}) and the fraction of interspike intervals (ISI) inferior to 1 ms (P_{ISI}). Isolation of Purkinje cells was generally better than for interneurons (mean P_{ISI} = 0.09% and 1.42%, respectively).

The procedures used do not allow the sorting of overlapping waveforms arising from occasional

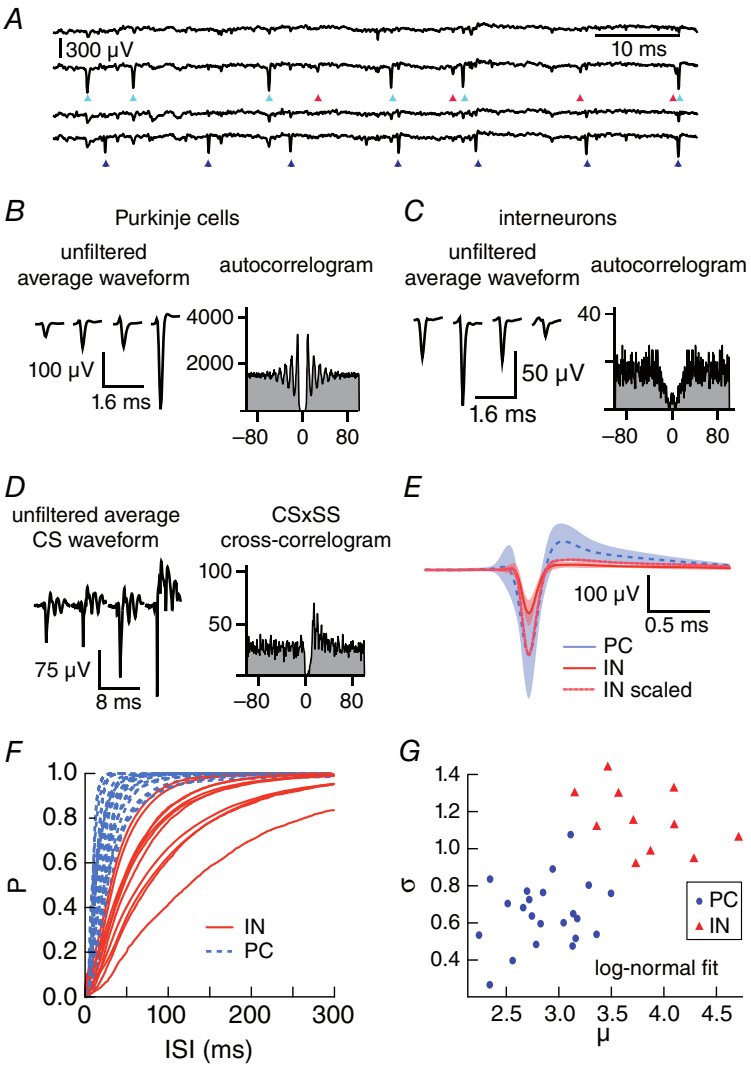

Figure 1. Isolation of Purkinje cells and molecular layer interneurons by tetrode recordings
A, example of raw traces. The four channels of the tetrode allow the isolation of one interneuron (red arrowheads; same cell as in *C*) and two Purkinje cells (light and dark blue arrowheads; dark blue same cell as in *B*). *B* and *C*, average (unfiltered) waveforms on the four channels and autocorrelograms of a Purkinje cell (*B*) and a molecular layer interneuron (*C*). *D*, complex spikes isolated for the Purkinje cell in *B* and cross-correlogram between complex spikes (CS) and simple spikes (SS), showing the characteristic pause after the occurrence of complex spikes. *E*, average unfiltered spike waveform of Purkinje cells (blue) and of interneurons (red). Interneuron spikes are slightly narrower and have a smaller rebound positivity, as seen when normalized by amplitude (red dashed line). *F* and *G*, distributions of ISIs for Purkinje cells and interneurons are distinct. *F*, cumulative distribution of ISIs for Purkinje cells (blue) and interneurons (red) and (*G*) fit of these distributions with a log-normal function: $f(x) = \frac{e^{-((\log(x)-\mu)^2/(2\sigma^2))}}{\sqrt{2\pi}\sigma x}$ (Pouzat and Chaffiol (2009). Bins in histograms *B*–*D*: 0.5 ms.

near-coincident spikes from two different units occurring within an interval of less than 0.5 ms (the width of the Purkinje cells spikes is less than 0.3 ms). As a result, spike train cross-correlations at submillisecond time lag were not computed in the present study.

The initial spike of a complex spikes has an amplitude profile over the tetrode channels similar to the simple spike of the same unit (de Solages *et al.* 2008). Thus, clustering pools simple and complex spikes from the same unit. To isolate the latter, their stereotypical waveform was obtained by averaging five to 10 complex spike waveforms selected by hand. Putative complex spikes were then detected as a slow component on the low-pass filtered (800 Hz) trace by measuring the difference between the minima of the potential in the 2.5 ms preceding and following each spike (detected on the high-pass filtered trace). These slow events were identified as complex spikes based on their similarity with the stereotypical waveform obtained previously, which was tested using Spearman rank order correlation coefficient computed for the 6 ms that followed the spike peak. The quality of isolation was confirmed by assessing the presence of a pause (10 ms or more) in simple spike firing of a Purkinje cell after a complex spike.

The present study combines recordings from anaesthetized rats (19 Purkinje cells and 10 interneurons; six recording sites in six rats) and from an awake rat (three Purkinje cells and one interneuron; one recording site). These cells behaved similarly and exhibited similar cross-correlations and therefore were pooled in the rest of the study.

In vitro electrophysiology

Slices of cerebellar vermis were prepared similarly to the method described in Isope & Barbour (2002). After the induction of anaesthesia with a ketamine–xylazine mixture, transcardiac perfusion of the rat with two cold, bubbled (95% O_2, 5% CO_2) solutions was performed. The first solution (150 ml) contained (in mM): 115 NaCl, 26 $NaHCO_3$, 3 KCl, 0.8 $CaCl_2$, 8 $MgCl_2$, 1.25 NaH_2PO_4, 10 D-glucose, 1 lidocaine-HCl and 1 ketamine-HCl. The second solution (100 ml) was identical except that sucrose (230 mM) replaced the NaCl. As soon as perfusion was under way, the abdominal aorta and/or the inferior vena cava were clamped, and the head of the rat was packed with ice. After perfusion, the rat was decapitated, the head was chilled over ice and the entire cerebellum was dissected out. Care was taken to avoid cutting or deforming the cerebellum. Sagittal slices (350 μm) of the cerebellar vermis were then cut using a 7000 smz slicer (Campden Instruments, Loughborough, UK) in an ice-cold solution containing (in mM): 230 sucrose, 26 $NaHCO_3$, 0.8 $CaCl_2$, 8 $MgCl_2$, 10 D-glucose, 1.25 NaH_2PO_4, 1 lidocaine, 1 ketamine and 0.05 D-APV. They were stored at 32°C in standard extracellular saline (bicarbonate-buffered solution), containing (in mM) 135 NaCl, 26 $NaHCO_3$, 3 KCl, 1.25 NaH_2PO_4, 2 $CaCl_2$, 1 $MgCl_2$ and 25 D-glucose, bubbled with 95% O_2/5% CO_2.

Recordings were performed at 32 ± 1°C in bicarbonate-buffered solution either under a BX51WI microscope (Olympus, Tokyo, Japan) equipped with a CoolSNAP EZ camera (Photometrics, Huntington Beach, CA, USA) controlled using microManager (Stuurman *et al.* 2007) and ImageJ (Abramoff *et al.* 2004) or under a Axioskop microscope (Carl Zeiss, Oberkochen, Germany) equipped with a 2000R Retiga camera (Qimaging, Surrey, BC, Canada). Whole-cell voltage and current-clamp recordings were obtained using either a Multiclamp 700B (Molecular Devices, Sunnyvale, CA, USA) or an Optopatch amplifier (Cairn Research, Faversham, UK) and optimal series resistance compensation (50–85% of 4–8 MΩ, typically) or capacitance neutralization as appropriate. For the experiments shown in Fig. 3, the pipette solution contained (in mM): 0.4 Na-GTP, 0.5 L-(–)-malic acid, 0.008 oxaloacetic acid, 0.18 α-ketoglutaric acid, 0.2 pyridoxal 5′-phosphate hydrate, 5 L-alanine, 0.15 pyruvic acid, 15 L-glutamine, 4 L-asparagine, 1 L-glutathione reduced, 10 Hepes, 4 KCl, 10 GABA, 2.1 Mg-ATP, 1.4 Na-ATP, 5 phosphocreatine-K_2, 0.5 K_3-citrate, 120 K-gluconate, 0.1 EGTA, 2.2 K_2-phosphate and 0.05 $CaCl_2$. For the experiments shown in Fig. 5, the pipette solution contained (in mM): 150 K-gluconate, 4 NaCl, 10 Hepes, 10 Mg-ATP and 13 biocytin pH-adjusted to 7.3 with KOH at 300 mosmol. Recordings were not corrected for the junction potential (estimated at 10 mV). Experiments were controlled using either WinWCP freeware (Strathclyde Electrophysiology Software, University of Strathclyde, Glasgow, UK) or Pclamp (Axon Instruments, Foster City, CA, USA).

Quantification of cross-correlograms

A cross-correlation histogram between two units is a measure of the number of spikes of the second unit occurring in a bin, b, centred on a given time shift, u, before/after a spike of the first unit. For a recording of length T, this cross-correlation histogram between units 1 and 2, termed $J_{12}(u)$, is therefore the number of spike pairs (i,j) of the two units occurring at times $(t_1(i),t_2(j))$ such that $|t_1(i) - t_2(j) - u| < b/2$.

To compute the significance in cross-correlation analysis, we used the standardized cross-covariance (Siapas *et al.* 2005). It is defined as $Q_{12}(u) = (J_{12}^{T,b}(u) - A)/\sqrt{A}$, with $A = N_1N_2b/T$, where N_1 and N_2 are the total numbers of spikes recorded from the units 1 and 2, Q_{12} is an estimate of the expected number of spikes in a bin for independent Poisson spike trains of the same intensities as the two units. The asymptotic distribution of the standardized cross-covariance is

thus approximately normal, $Q_{12}(u) \sim N(\mu = 0,\ \sigma^2 = 1)$. Significant modulation was assumed when $|Q_{12}(u)| > z_{crit}$ and tested on the 60 × 1 ms bins of our ±30 ms cross-correlation histogram. The level of significance ($\alpha = 0.05$) was thus divided by 60 yielding a critical Z-value of 3.34. Normalized cross-correlograms were obtained by dividing the observed cross-correlogram by A, the expected number of spikes per bin.

Phase-locking using the spike-triggered average

For each neuron, we calculated the spike-triggered average of the extracellular potential. We compared the peak found in the spectra of the spike-triggered averages with the peak found in the spectrum of the local field potential for the different recordings. Spectral density estimates of the continuous signal were obtained with Welch's method with windows of 4096 points (164 ms) for the spike-triggered averages and local field potential signal. The peak frequencies were obtained from a fit of the power spectrum with a Lorentzian curve (chosen because of its appropriate shape) added to a linear trend.

Recurrence-time analysis

The recurrence-time analysis that we developed is inspired by Johnson & Kiang (1976). It describes the distribution of latencies to the first Purkinje cell spike after the interneuron spike, knowing the time interval between the last spike of the Purkinje cell and the interneuron spike. This allows us to examine the inhibition induced by the interneuron at the same time as taking into account the firing history of the Purkinje before the interneuron (a parameter not taken into account by Johnson & Kiang, 1976).

From spike trains of the interneuron and the Purkinje cell, we compute, for each interneuron spike, the intervals ('recurrence times') from the previous Purkinje cell spike, t_{back} (Fig. 4*A*, blue), and to the next spike, $t_{forward}$ (Fig. 4*A*, green). Histograms of these values of recurrence times provide a rough estimate of the corresponding probability density function P_{back} and $P_{forward}$. If the interneuron has no action on the Purkinje cell firing (null hypothesis), it should be possible to predict the distribution of Purkinje cell firing after the interneuron with the knowledge of when it fired before (P_{back}) and of the Purkinje cell firing ISI probability density function P_{ISI}. This prediction is close to a convolution of P_{back} and P_{ISI} (eqns (1) and (2)). An estimate of this predicted distribution was computed by discretization (we used a bin of 1 ms) and use of the empirical estimates of P_{back} and P_{ISI}.

The estimate of the prediction distribution can be compared with the observed distribution (Fig. 4*B* and *C*). The difference between the observed and expected distributions provides an estimate of the time course of the effect of the interneuron on the Purkinje cell (Fig. 4*D*):

$$P_{forward}^{[predict]}(t_0) = \int_{t>0} P_{back}(t).P_{ISI}(ISI = t + t_0 | ISI \geq t).dt \quad (1)$$

which can be written as:

$$P_{forward}^{[predict]}(t_0) = \int_{t>0} P_{back}(t).\frac{P_{ISI}(ISI = t + t_0)}{\int_{i\geq t} P_{ISI}(i).di}.dt \quad (2)$$

An important benefit of these approach is that the estimate of the expected distribution $P_{forward}^{[predict]}$ is smooth because it is obtained by an integration. It is also possible to build confidence intervals, according to the binomial probability: to each bin centred in h with a width dh (we used $dh = 1$ ms) of the histogram of $t_{forward}$ corresponds a probability of realization $p(h) = P_{forward}(h)^{[predict]}.dh$. N realizations should produce in average $N.p(h)$ values in the bin centred in h with a standard deviation $s(h) = \sqrt{N.p(h)(1-p(h))}$. It is then possible to build a confidence interval by defining a significance level α which provides a Z_{critic} and a confidence interval $Z_{critic}.s(h)$. Differences between observed and predicted values of the distribution of $t_{forward}$ falling out of the confidence interval may then be identified and counted (Fig. 4*E*).

The intersection point between the predicted and the observed $t_{forward}$ distributions, corresponding to the zero-crossing point of the residuals distribution, was used to define the duration of the diminution of Purkinje cell firing probability. The strength of inhibition was quantified by comparing the integral of the distributions for the delay values during this period, and calculating the percentage of the observed integral compared to the predicted one.

To study the influence of the interneuron synchrony on inhibition strength, we used recordings in which more than one interneuron had been isolated (three recordings containing two, two and three interneurons, $n = 11$ Purkinje cells). For each Purkinje cell–interneuron pair, the inhibition strength was defined as the integral value of negative residuals.

Delayed-spike curve (DSC)

To compute the DSC (Fig. 5), we need to estimate, for each interval t_{back} (between a Purkinje cell spike and a following interneuron spike), how much the average of the observed interval $t_{forward}$ (between the interneuron spike and the following Purkinje cell spike) deviates from the prediction that can be made based on the sole distribution of ISIs.

We first computed the observed averaged value of time intervals from an interneuron spike to the next Purkinje spike $<t_{forward}(t_{back})>^{[observed]}$, using 3 ms time bins for

t_{back} values. To compute the expected $<t_{forward}(t_{back})>$ for each $t_{back} > 0$, we either simply took the average of Purkinje cell ISIs larger than t_{back}:

$$<t_{forward}\,(t_{back})>^{[\text{expected from ISI}]} = \frac{\int_{i>t_{back}} i.P_{ISI}(i).di}{\int_{i>t_{back}} P_{ISI}(i).di} - t_{back} \quad (3)$$

or estimated the average $<t_{forward}(t_{back})>$ for each t_{back} produced by replacing the interneuron spikes with random spike trains with the same ISI distribution and length; such a computation was repeated 10 times to estimate a $<t_{forward}(t_{back})>^{[\text{expected from random}]}$. The DSC was estimated as the difference between either of these two quantities:

$$DSC\,(t_{back}) = <t_{forward}\ (t_{back})>^{[\text{observed}]} - <t_{forward}\,(t_{back})>^{[\text{expected}]} \quad (4)$$

A linear fit was then performed on DSC values to provide a first-order estimate of the time-dependence of the effect of interneurons on Purkinje cells. Both methods yielded similar estimates of the slope of the DSC.

Exponential tail of the ISI distribution

To study the distribution of interspike intervals, the ISI histogram was first constructed (bin = 1 ms). Using a linear fit on the logarithm of the ISI histogram count, single exponential fits were performed on the tail of the histogram, starting from the eight last values of the tail (dropping the parts of the histogram with spike counts inferior to 10 values per bin; indicated in grey in Fig. 6*B*), and then increasing the number of the values used for the fit: nine last values, then 10 last values, etc. For each of these fits, the SD of the residuals was computed, and the fit with the lowest standard deviation of residuals was considered as the one identifying the longest part of ISI tail optimally described with a single exponential; the beginning of this tail signals the 'memory time' of the cell (Ostojic, 2011). Care was taken to perform the fits on parts (>90 s) of the recordings with a stable firing rate because fluctuations in the average firing rate shall modify the ISI distribution.

Model

The interneuron was modelled as a single-compartment exponential integrate-and-fire model, in which the dynamics of the membrane potential are given by:

$$C\frac{dV}{dt} = -g_l\,(V - V_{rest}) + g_l\Psi\,(V) + I_{bkg}^{IN} \quad (5)$$

The membrane time constant was $C/g_l = 20$ ms, the resting potential $V_{rest} = -65$ mV and the $g_l\Psi$ and I_{bkg}^{IN} currents are defined below.

The Purkinje cell was modelled as a two-compartment exponential integrate-and-fire model which was found to account well for the very fast response of Purkinje cells (Ostojic *et al.* 2015). We refer to the two compartments as 'somatic' and 'dendritic'. Dynamics of the membrane potentials V_s and V_d in the two compartments are given by:

$$\begin{aligned} C_s\frac{dV_s}{dt} &= -g_sV_s + g_j\,(V_d - V_s) + (g_s + g_j)\Psi\,(V) \\ &\quad + I_{syn} + I_{bkg}^{PCs} \\ C_d\frac{dV_d}{dt} &= -g_dV_d + g_j\,(V_s - V_d) + I_{bkg}^{PCd}. \end{aligned} \quad (6)$$

Values of the capacitances and conductances of the two compartments were $C_s = 30$ pF, $C_d = 1500$ pF, $g_s = 0.6$ nS and $g_d = 30$ nS, whereas the junctional conductance was $g_j = 200$ nS.

The interneuron compartment and the somatic compartment of the Purkinje cell contain an exponential spike-generating mechanism Ψ (Fourcaud-Trocmé *et al.* 2003; Badel *et al.* 2008):

$$\Psi\,(V) = \Delta_T \exp\left(\frac{V - V_T}{\Delta_T}\right). \quad (7)$$

The normalization of Ψ is chosen in Eqns (5) and (6) such that V_T is the spike threshold. Namely, once the membrane potential crosses the threshold V_T, it diverges to infinity in finite time as a result of this exponential current. This divergence represents the firing of an action potential. Following the divergence, the membrane potential is reset to a value V_r after a refractory period τ_{rp}. In the two compartment model, following the action potential, the dendritic compartment was hyperpolarized by an amount β_d. The parameter Δ_T quantifies the sharpness of the action potential initiation. For the Purkinje cell, $\Delta_T \approx 0.75$ mV (Rieubland *et al.* 2008) and this value was used in both interneuron and Purkinje cell models. The other parameters were $V_T = -50$ mV, $V_r = -60$ mV, $\tau_{rp} = 1$ ms and $\beta_d = 0.5$ mV.

The somatic compartment of the Purkinje cell model received GABAergic synaptic inputs I_{syn} from the interneuron modelled as a delayed difference of exponentials:

$$I_{syn}\,(t) = g_{syn}(V_s - V_{syn})\left(\exp\left(-\frac{t - \tau_l}{\tau_d}\right) - \exp\left(-\frac{t - \tau_l}{\tau_r}\right)\right)\frac{\tau_r}{\tau_d - \tau_r}\left(\frac{\tau_r}{\tau_d}\right)^{\frac{-\tau_d}{\tau_d - \tau_r}}. \quad (8)$$

where the peak conductance ($g_{syn} = 0.4$ nS), latency ($\tau_l = 1.5$ ms), rise time ($\tau_r = 0.5$ ms) and decay time ($\tau_d = 3$ ms) were taken from *in vitro* electrophysiological measurements of spontaneous inhibitory currents in

Purkinje cell of adult rats (de Solages *et al.* 2008). The chloride reversal potential was taken as $V_{syn} = -70$ mV.

The interneuron and the two compartments of the Purkinje cell model received fluctuating inputs I_{bkg}^{IN}, I_{bkg}^{PCs} and I_{bkg}^{PCd} mimicking background synaptic activity. These fluctuating inputs were defined as:

$$I_{bkg}^{IN} = \mu_{IN} + \sqrt{1 - f_{IN}}\sigma_{IN}\eta_{IN}(t) + \sqrt{f_{IN}}\sigma_{IN}\eta_{common}(t) \quad (9)$$

$$I_{bkg}^{PCs} = \mu_{PC} + \sqrt{1 - f_{PC}}\sqrt{\frac{C_s}{C_s + C_d}}\sigma_{PC}\eta_{PCs}(t) + \sqrt{f_{PC}}\sqrt{\frac{C_s}{C_s + C_d}}\sigma_{PC}\eta_{common}(t) \quad (10)$$

$$I_{bkg}^{PCd} = \sqrt{1 - f_{PC}}\sqrt{\frac{C_d}{C_s + C_d}}\sigma_{PC}\eta_{PCd}(t) + \sqrt{f_{PC}}\sqrt{\frac{C_d}{C_s + C_d}}\sigma_{PC}\eta_{common}(t). \quad (11)$$

Here, μ_{IN} and μ_{PC} represent the mean fluctuating input to the interneuron and to the Purkinje cell. The terms η_{IN}, η_{PCs}, η_{PCd} and η_{common} are uncorrelated Ornstein–Uhlenbeck stochastic processes given by:

$$\tau_n d\eta_i(t)/dt = -\eta_i(t) + \sqrt{\tau_n}\xi_i(t) \quad (12)$$

where $\xi_i(t)$ are white-noise processes of zero mean and unit variance, and $\tau_n = 1$ ms. The terms proportional to η_{common} represent the shared fluctuating input between the interneuron and the two compartments of the Purkinje cell. The parameters f_{IN} and f_{PC} represent the fraction of the variance as a result of common inputs in the interneuron and the Purkinje cell. The variances of the fluctuating inputs to the two compartments of the Purkinje cell model were moreover proportional to the areas of the compartments. The means μ_{IN} and μ_{PC}, and SDs σ_{IN} and σ_{PC} of the total fluctuating inputs were adjusted to reproduce the observed firing rates and coefficients of variation of interspike intervals.

The phase–response data shown in Fig. 5*G* were obtained by simulating the above models of interneuron and Purkinje cell dynamics in absence of shared inputs, and applying the same analysis as for experimental data.

The illustration of the mechanism in Fig. 6 was generated using a single compartment leaky integrate-and-fire model with a membrane time-scale of 20 ms and white-noise fluctuating inputs (Ostojic, 2011). The mean ± SD values of these fluctuating inputs were fixed to reproduce a firing rate of 30 Hz and coefficients of variation of 0, 0.22 and 0.75. Poisson-distributed instantaneous current inputs were added to estimate the phase–response curve.

Table 1. Firing and spike waveform properties for Purkinje cells (PC) and interneurons (IN)

Mean ± SEM	PC ($n = 22$)	IN ($n = 11$)	*P*-value
Rate	48.9 ± 4.19 Hz	14.9 ± 1.81 Hz	$<1 \times 10^{-4}$
Spike amplitude	125 ± 12 μV	62 ± 6 μV	0.002
FWHM	178 ± 7 μ s	137 ± 5 μs	0.0003
CV ISI	0.81 ± 0.08	0.93 ± 0.03	0.03
CV log(ISI)	0.23 ± 0.01	0.30 ± 0.02	0.006
CV2 ISI	0.64 ± 0.03	0.89 ± 0.02	$<1 \times 10^{-4}$
entropy	6.97 ± 0.09	7.66 ± 0.04	$<1 \times 10^{-4}$
ISI location	2.87 ± 0.07	3.82 ± 0.14	$<1 \times 10^{-4}$
ISI scale	0.66 ± 0.04	1.14 ± 0.05	$<1 \times 10^{-4}$

Spike amplitude is calculated from the baseline on the channel with maximal amplitude. FWHM, full-width at half-maximal amplitude of the spline-interpolated waveform; CV, coefficient of variation. CV2 ISI is defined by the equation: $\langle 2.\frac{ISI_{i+1} - ISI_i >}{ISI_{i+1} + ISI_i >} \rangle$ (Holt *et al.* 1996), entropy: entropy of the log(ISI) distribution, computed as in Van Dijck *et al.* (2013); ISI location/scale, location and scale of the log-normal distribution fitted to the empirical interspike interval distribution.

Statistical analysis

Values in the text are given as the mean ± SEM unless specified. Tests were performed using a two-sample Student's *t* test.

Results

Tetrode recordings in the Purkinje cell layer enable the isolation of Purkinje cells and molecular layer interneurons

Simultaneous multiple single-unit recordings were obtained in the vicinity of the Purkinje cell layer in the cerebellar vermis using tetrodes (see Methods). In a few instances (~5% of our Purkinje cell layer recordings) that we report in the present study, two types of units were distinguishable (Fig. 1*A*): (1) fast firing units (20–60 Hz) (Table 1), with an autocorrelogram that exhibits a typical central trough (Fig. 1*B*), and with the characteristic properties of Purkinje cells recorded in the Purkinje cell layer (Ruigrok *et al.* 2011; Gao *et al.* 2012; Van Dijck *et al.* 2013), and (2) slower units with flatter autocorrelograms (Fig. 1*C*). The identity of the fast units was confirmed by isolating complex spikes in a subset of them (Fig. 1*D*).

The second type of unit ($n = 11$) had a slightly narrower spike and a smaller spike amplitude, (Fig. 1*E* and Table 1), a flatter autocorrelogram than Purkinje cells (Fig. 1*C*), a wider distribution of ISIs (Fig. 1*F* and *G* and Table 1) and was devoid of complex spikes. These units were only detected in a limited subset of recordings, possibly as a result of the small amplitude of their spikes, which required the exact positioning of the electrode in the vicinity of the

cell and an excellent signal/noise ratio, or their sensitivity to anaesthetics (in one recording, we transiently raised the isoflurane level from 0.5% to 1%, which caused a reversible extinction of the second type of unit). The recording location, close to the Purkinje cell layer, and the firing statistics of these units are compatible with properties distinctive of morphologically identified basket cells in the cerebellum (Ruigrok *et al.* 2011; Van Dijck *et al.* 2013). They are therefore referred to as interneurons throughout the present study.

Interneurons exhibit asymetric cross-correlograms with the Purkinje cell population

To study the changes in firing probability of one cell around the spike of another cell, we examined their cross-correlograms. Cross-correlograms between Purkinje cells exhibit positive correlations at ±1 ms and ±4–6 ms (n = 43) (Fig. 2*A*–*C*), indicative of a population oscillations at ∼200 Hz (de Solages *et al.* 2008). By contrast, cross-correlograms between interneurons (Fig. 2*D*–*F*) did not display such fast oscillations

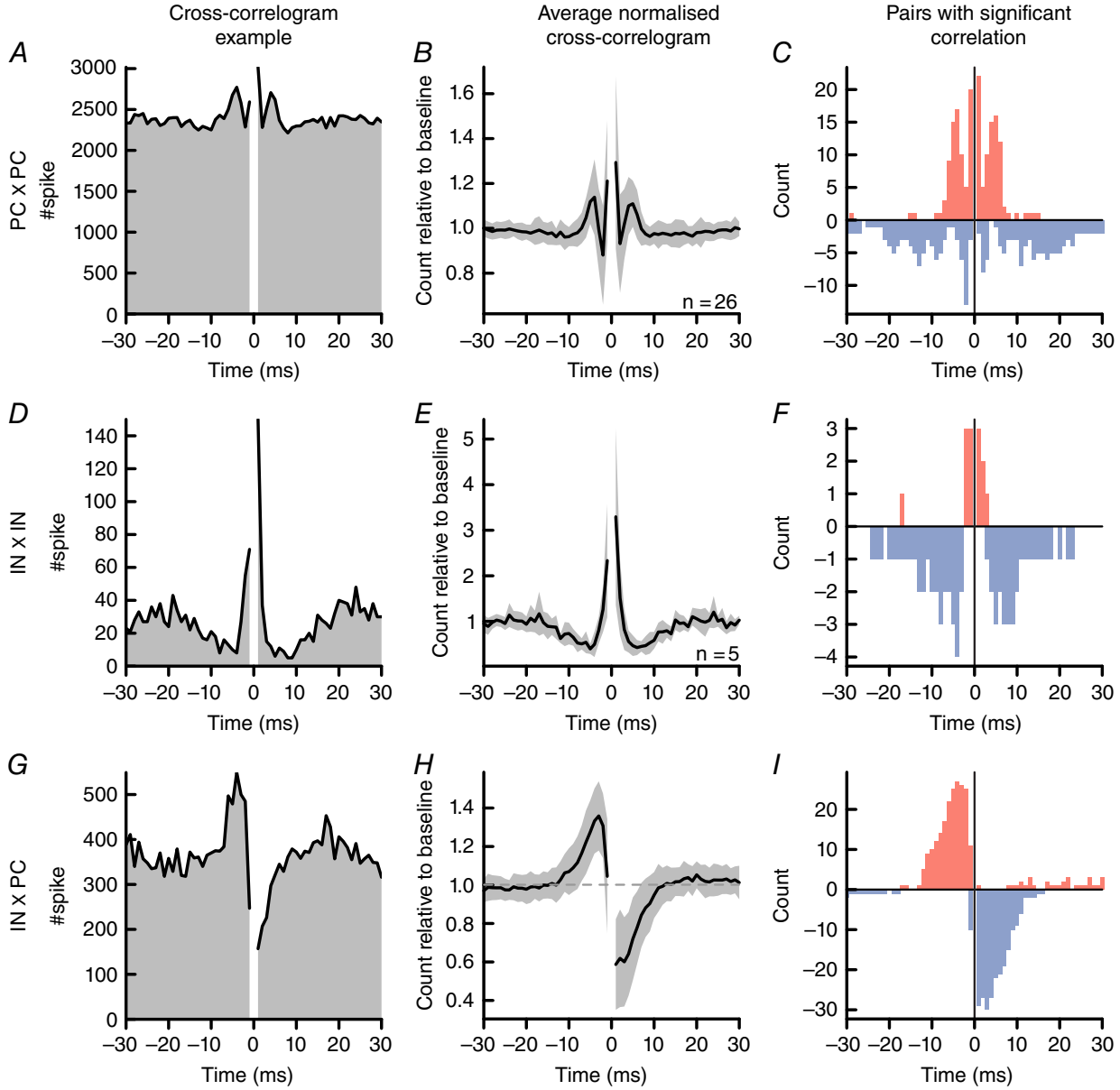

Figure 2. Short-term correlations between recorded cells
A, *D* and *G*, specimen cross-correlograms of two neighbouring neurons recorded simultaneously from a single tetrode, average normalized cross-correlograms (*B*, *E* and *H*) and number of pairs with significant correlations for each bin (*C*, *F* and *I*, positive in red, negative in blue) for Purkinje cell pairs (*A*–*C*), interneuron pairs (*D*–*F*) and interneuron–Purkinje cell pairs (*G*–*I*). Bin = 1 ms. For the missing value at 0, see Methods.

but revealed a ∼3 ms large peak of positive correlations around 0 surrounded by ∼15 ms troughs, indicative of near-synchronous discharge. This pattern is similar to that reported previously for pairs of molecular layer interneurons *in vitro* (Mann-Metzer & Yarom, 1999). Interneurons are connected by electrical and chemical synapses (Kim *et al.* 2014; Rieubland *et al.* 2014). Although the former have been shown to generate the central positive correlation (Mann-Metzer & Yarom, 1999), lateral troughs may also result from synaptic cross-inhibition.

Cross-correlograms between simultaneously-recorded interneurons and Purkinje cells (with interneuron spikes at $t = 0$) often displayed a trough lasting ∼7 ms ($n = 36$) (Fig. 2*G–I*), indicative of a reduction in the average Purkinje cell spike count after the interneuron spikes. Interestingly, the probability of Purkinje cell firing tended to increase before the interneuron spike, as revealed by the peak before 0 in the cross-correlogram. We never observed pairs of peaks at ±4–5 ms as in Purkinje cell–Purkinje cell cross-correlograms. Thus, the interneurons recorded appear to inhibit Purkinje cells but do not exhibit, in their cross-correlograms, the 200 Hz ripples (i.e. 4–5 ms side peaks around a central peak) found between cells embedded in the fast population oscillation (de Solages *et al.* 2008).

Molecular layer interneurons mediate feed-forward inhibition

In our recordings, molecular layer interneuron action potentials were generally preceded by an increase in Purkinje cell activity (∼30% excess of Purkinje cell spikes) and followed by a decrease of activity (∼30% deficit of Purkinje cell spikes) (Fig. 2*G–I*).

To quantify this phenomenon, for each time bin, the fraction of all pairs of units with either positive or negative significant correlation was computed (Fig. 2*I*). In the [–15, –1] ms window, a significant excess of Purkinje cell spikes before interneuron action potentials was present (for at least one 1 ms time bin) in 30/36 (83%) pairs. Similarly, a significant reduction of Purkinje cell firing in the [+1, +15] ms window was observed in 31/36 (86%) pairs.

In most pairs where inhibition of the Purkinje cell was seen, there was an increased spiking of Purkinje cell before the interneuron spikes (Fig. 3*A*) and we next examined whether this increase resulted from a disinhibition. Interneurons indeed have long ISIs (Fig. 1*F*) and tend to be synchronous (Fig. 2*D–F*). Their spikes might thus be preceded by a period during which interneurons have a reduced firing probability. This would cause a partial disinhibition and could explain the observed increase in Purkinje cell spike count. To test this hypothesis, we selected interneuron spikes that were preceded and followed by a period of 50 ms without discharge, therefore removing any change in average inhibition that could be linked to the previous or next spikes (Fig. 3*B*). Even in this case, Purkinje cells increased their firing immediately before the interneuron discharge, suggesting that Purkinje cells share common excitatory inputs with interneurons that inhibit them.

To assess the existence of shared excitatory inputs, we simultaneously recorded, in sagittal slices of cerebellar vermis, Purkinje cells voltage clamped in the whole-cell configuration, as well as molecular layer interneuron activity using loose-cell attached recording. The average Purkinje cell current triggered on spontaneous interneuron spikes displayed an average waveform (Fig. 3*C*) with a time course strikingly similar to the cross-correlogram obtained *in vivo* (Fig. 3*B*). Indeed, interneuron spikes were preceded by an inward (excitatory) current of -1.2 ± 0.3 pA (different from 0; $P < 0.001$, $n = 30$) and followed by an outward (inhibitory) current 3.9 ± 0.8 pA ($P = 2 \times 10^{-5}$, $n = 30$). The onset of the outward current is masked by a ∼1 pA peak centred around 0 (i.e. around the peak of the action potential in the interneuron). This peak probably has two origins: a small artefactual coupling between the two recording channels (for another example of such coupling, see Ko *et al.* 2011) and the coupling between the basket and the Purkinje cell soma that it surrounds (Blot & Barbour, 2014).

The synaptic outward (inhibitory) current following the interneuron spike was preceded by an inward current in the Purkinje cell, indicating that events producing the interneuron spikes were associated with excitation of the Purkinje cell. The biphasic pattern observed in the cross-correlograms thus appears to be produced by a shared excitatory input followed by inhibition of the Purkinje cell by the interneuron.

A simple model of feed-forward inhibition reproduces the shape of the cross-correlogram

We aimed to simulate the features of interactions between Purkinje cells and interneurons using a simplified model (Fig. 3*E–F*) to test whether feed-forward inhibition could indeed induce this pattern of correlations. Purkinje cells and interneurons were modelled as leaky integrate-and-fire neurons with two (de Solages *et al.* 2008; Ostojic *et al.* 2015) and one compartment, respectively. Because recorded interneurons are probably basket cells (see Discussion), synapses between interneurons and Purkinje cells were implemented on the somatic Purkinje cell compartment only. Excitatory currents from granule cell inputs were produced in both cells by partially common fluctuating inputs, the intensity of which was adapted to reproduce the firing rate and the coefficient of variation of ISIs found in our recordings.

Cross-correlograms obtained by this model reproduced qualitatively the data observed *in vivo* (Fig. 3*F*, blue), with an initial co-excitation followed by an inhibition

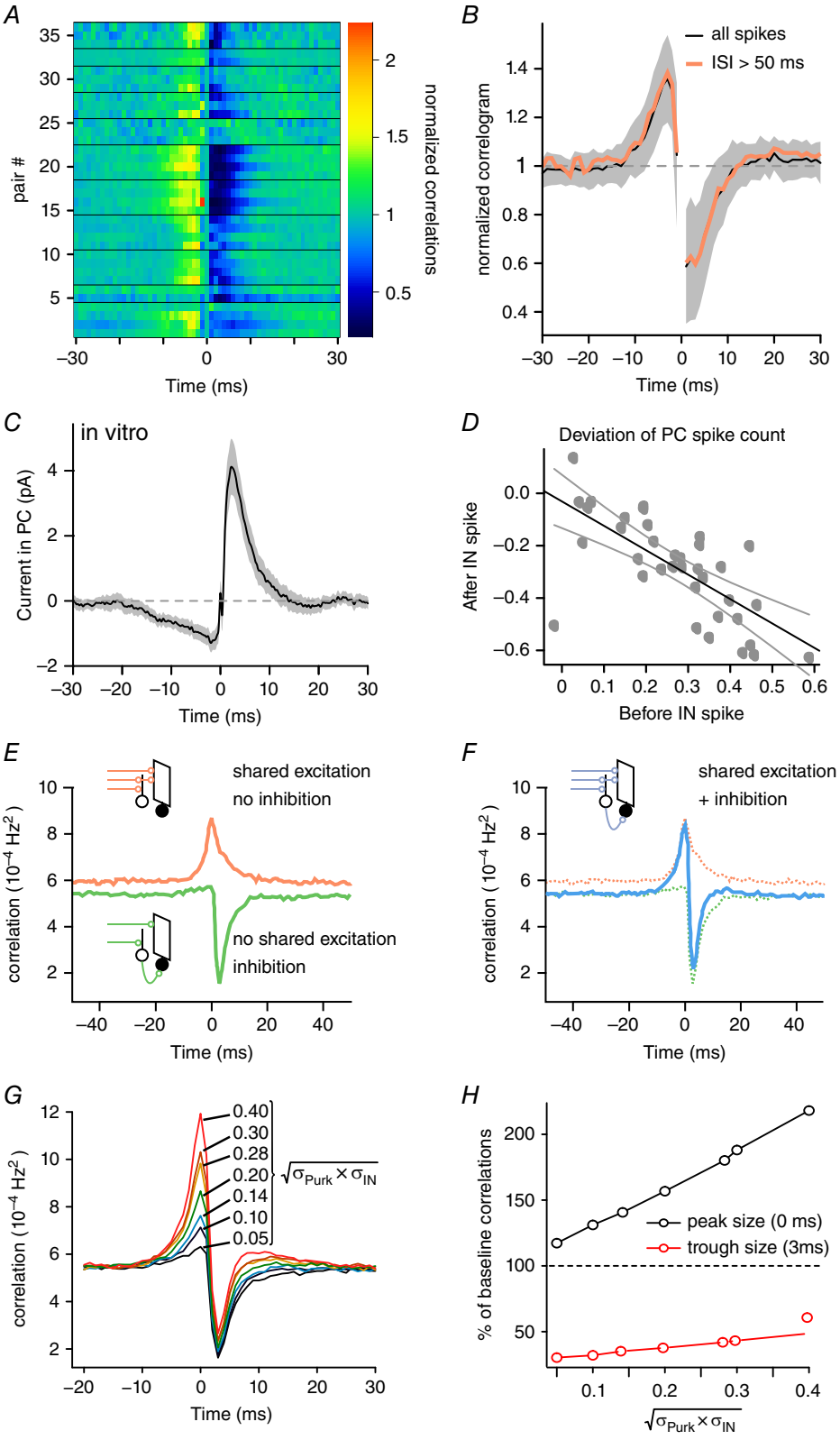

Figure 3. Molecular layer interneurons mediate feed-forward inhibition
A, normalized cross-correlogram for all interneuron–Purkinje cell pairs. Each recording session is separated by a horizontal line. The cross-correlogram of each pair was normalized (as in Fig. 2*H*), and is represented by a single line on the image with the colour corresponding to the value of the cross-correlogram at each time point. *B*, correlogram with all interneuron spikes (black) or with only interneuron spikes preceded and followed by

of the Purkinje cell. This pattern was dependent on feed-forward inhibition because driving the two cells with entirely independent fluctuating input processes abolished the co-excitation, leaving only the inhibition (Fig. 3*E*, green). Conversely, the effect of shared inputs can be assessed by removing the synapses between the Purkinje cell and interneurons (Fig. 3*E*, red) and reveals a broad synchronization, of which the late phase is normally hidden by inhibition. The correlogram corresponding to feed-forward inhibition can be obtained by summing the correlograms corresponding, respectively, to a direct inhibitory connection and to shared inputs (Ostojic *et al.* 2009).

Varying the amount of shared excitation changes the amplitude of the positive peak in the cross-correlograms (Fig. 3*G–H*); the size of this peak essentially depends on the square root of the product of the fraction of excitatory inputs of each cell that are shared with the other cell (Ostojic *et al.* 2009) and values of this parameter between 0.1 and 0.8 produce an excess of ∼15% to ∼120% correlations (peak correlation divided by the baseline correlation value) between the cells (Fig. 3*H*).

In this model, the amplitudes of the excitatory and inhibitory phases of the correlogram are set by independent parameters (strength of common inputs and strength of inhibition). Interestingly, this independence was not observed in our *in vivo* recordings, where the average amplitudes of these two phases were correlated ($P = 2 \times 10^{-6}$) (Fig. 3*A* and *D*). This suggests that the strength of inhibition was matched to the strength of shared excitation *in vivo*.

Reduced Purkinje cell spike count after interneurons spike in cross-correlogram corresponds to inhibition

As shown above, discharges of Purkinje cells and interneurons are coupled and interneuron spikes are generally preceded by an increased discharge probability of the Purkinje cells, which is attributed to shared excitation. We interpreted above the reduction in Purkinje cell spike count after the interneuron spikes as the result of inhibition. However, because Purkinje cell ISIs are rarely shorter than 7 ms, a reduction in the Purkinje cell spike count is expected after they have been active. A common excitation of Purkinje cells and interneurons leading to a preferential sequence of activation of Purkinje cells before interneurons might therefore account for the reduced Purkinje cell spike count after the interneuron spikes, and thus explain the observed correlation between the size of peaks and troughs of Purkinje cell spike counts, respectively, before and after interneurons spikes (Fig. 3*D*).

To assess quantitatively how much of the reduced Purkinje cell spike count after the interneuron spike is a result of inhibition (*vs.* explained by the recent Purkinje cell firing history), we designed a method derived from the recurrence-time method from Johnson and Kiang (1976), which takes into account the firing history of the Purkinje cell before the interneuron spike, and compares the observed distribution of Purkinje spikes after the interneuron with the expected distribution if the interneuron had no effect. Briefly, we computed the distribution of Purkinje cell interspike intervals (ISIs) (i.e. the distribution of latencies between successive Purkinje cell spikes; Fig. 4*A* and *B*, black). Assuming the interneuron has no effect on the Purkinje cell, we can produce an estimate of the expected distribution of the latencies between the interneuron action potential and the first Purkinje cell spike following it (Fig. 4*B* and *C*, orange, expected t_{forward}). This is achieved by combining (an operation close to a convolution, see Methods) the Purkinje cell ISI distribution and the distribution of time intervals between interneuron action potentials and the previous spike of the Purkinje cell (Fig. 4*A* and *B*, blue, t_{back}). A confidence interval for this smooth estimate can be easily derived (see Methods). This estimate can then be compared with the observed distribution of t_{forward} to reveal the actual effect of the interneuron (Fig. 4*A* and *C*, green). The subtraction

ISIs longer than 50 ms (red). Note that the red line is located slightly above the black line, indicating a slightly higher firing probability of Purkinje cell spikes before and after the interneuron if no interneuron spike takes place during that period of time. *C*, average of Purkinje cell current, triggered on spontaneous interneuron spikes, recorded by whole cell patch-clamping *in vitro* reveals incoming excitation before the inhibitory current. *D*, the increase in Purkinje cell normalized spike count before and the decrease after the interneuron spike (*in vivo* data, averaged over the ±2–8 ms window) are correlated (normalization as in *A*). *E–F*, correlations for various connectivity patterns in a simple model of interneuron + Purkinje cell (see Methods) *y*-axis: Purkinje cell spike count per interneuron spike (bin = 0.5 ms). *E*, in a model with an inhibitory connection between the Purkinje cell and the interneuron, a monophasic reduction of firing (green) is observed. Injecting shared common noise inputs in a interneuron – Purkinje cell pair that is not synaptically connected produces a broad synchronization of the Purkinje cell and interneuron (orange). *F*, a pattern of cross-correlogram similar to that observed *in vivo* (*B*) is found when the interneuron and Purkinje cell receive both common and independent noise and the interneuron inhibits the Purkinje cell (blue). *G*, cross-correlograms of simulated spike trains computed for varying amounts of shared inputs; the numbers correspond to the square root of the product of the fraction of shared inputs in each cell (e.g. 0.28 corresponds to 40% and 20% of shared inputs in the cells $\sqrt{0.4^*0.2}$). *H*, amplitude of the peak and trough of the simulated cross-correlograms as a function of the square root of the product of the fraction of shared inputs in each cell ($\sqrt{\sigma_{\text{Purk}}{}^*\sigma_{\text{IN}}}$). Grey shadings in *B* and *C* are the SEM.

of the two (observed – expected) indicates a departure from the null hypothesis (an absence of modulation of the Purkinje cell by the interneuron) and revealed significant early negative and late positive modulations (Fig. 4*D*, red and blue, respectively,).

Recurrence-time analysis thus confirmed that interneurons recorded inhibit Purkinje cells (Fig. 4*E*–*G*). The inhibition reduces the spike occurrence by 46.8 ± 3.2% (reduction at maximal inhibition, average inhibition profile in Fig. 4*F*) (n = 32). This inhibition lasted 8.5 ± 0.5 ms (Fig. 4*F*; its onset could not be resolved as a result of difficulties in sorting spikes separated by less than 1 ms; see Methods). The reduction of Purkinje cell spike count after the interneuron discharge is thus not only a result of co-excitation (and sequential firing) of the two cell types but also a genuine inhibition.

Molecular layer interneurons are coupled by gap junctions (Sotelo & Llinás, 1972), which synchronize their firing *in vitro* (Mann-Metzer & Yarom, 1999) and probably also contribute to the synchrony observed *in vivo* (Fig. 2*D*–*F*). The coincident inhibitory inputs of multiple interneurons should enhance the inhibition. Using recordings with multiple interneurons (three recordings containing two, two and three interneurons, n = 11 Purkinje cells), we quantified this phenomenon by selecting interneuron spikes that were synchronous (in a 3 ms window). These spikes represented only a minority of the total number of spikes (mean ± SD, 13 ± 6%). We then compared the changes in Purkinje cell spike occurrence probability (Fig. 4*D*) following synchronous or non-synchronous interneuron spikes (Fig. 4*G*). The inhibition was stronger when spikes

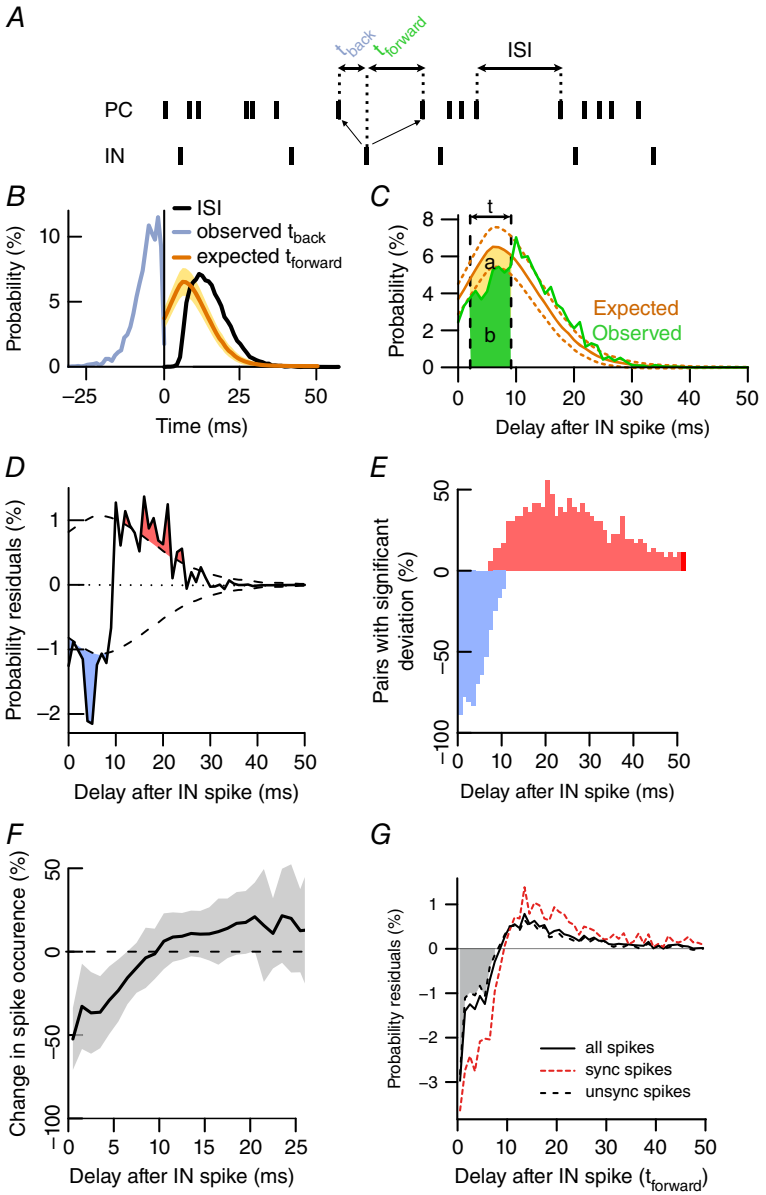

Figure 4. Interneurons modulate Purkinje cell firing probability
A–*C*, principle of analysis. *A*, schematic Purkinje cell and interneuron spike train. For every interneuron spike, we call t_{back} the time between the last Purkinje cell and the interneuron spike and $t_{forward}$ the time between the interneuron spike and the next Purkinje cell spike. The Purkinje cell ISI distribution (*A* and *B*, black) is used to predict the expected latency after the interneuron spike (*B* and *C*, prediction of $t_{forward}$, orange), knowing the time subsequent to the last Purkinje cell spike (*A* and *B*, t_{back}, blue). This prediction is compared with the observed distribution of latencies to the first Purkinje cell spike after the interneuron spike (*A* and *C*, $t_{forward}$, green).
C, example of observed (green) and expected ± SEM (orange respectively full and dashed lines) $t_{forward}$ distributions for one interneuron–Purkinje cell pair. The observed distribution is significantly lower than that expected for delay values in the range *t*. The strength of inhibition can be defined as the difference of probability for these delays (orange area a between the two curves), divided by the integral of the expected distribution of intervals for the same delays ($a + b$). *D*, difference between the two distributions shown in *C*, revealing the delays after the interneuron spikes at which the Purkinje cell fires significantly less (blue) or more (red) than expected. *E*, histogram of percentage of pairs showing significant modulations at each time bin. *F*, strength of modulation expressed as the percentage change in Purkinje cell spike occurrence from expected value (black line; SEM in grey). *G*, average probability residuals (as in *D*) after all (black, continuous line), non-synchronous (black, dashed line) or only synchronous (red) interneuron spikes for recordings where two interneurons could be recorded simultaneously. The increase in inhibition strength by synchrony is calculated by comparing the negative residuals obtained with the two conditions. Data are from 36 pairs from seven recording sites in seven rats.

were synchronous [integral of the negative residuals for interneuron synchronous spikes was, mean ± SD: 105 ± 17%, median 54%, significantly bigger ($P = 0.006$) than for all interneuron spikes, and was mean ± SD: 179 ± 66%, median 72%, significantly bigger ($P = 0.002$) than for non-synchronous interneuron spikes, $n = 13$ pairs interneuron–Purkinje cell]. The duration of inhibition, measured as the intersection of the residual curves with zero, was however not significantly changed (ratio with unsynchronous spikes, mean ± SD: 18 ± 14%, bigger, $P = 0.20$; all spikes: 5.2 ± 30%, bigger, $P = 0.9$). Thus, interneuron synchronization did not significantly prolong the inhibition of Purkinje cells but increased its strength by a factor 2 during the same ∼8 ms period.

High levels of synaptic inputs allow molecular layer inhibition to be independent of Purkinje cell firing cycle

Purkinje cells are intrinsically rhythmic and are sometimes considered as oscillators, and synaptic inputs can be viewed as perturbation applied to the oscillation. In this context, a much studied quantity is the phase–response curve (Ermentrout & Terman, 2010), which assesses changes in the impact of a perturbation as a function of its time in the firing cycle. *In vitro*, current injections in the somatic compartment of Purkinje cell can produce an inhibition of variable duration, depending on the phase of the Purkinje cell firing cycle at which they occur. For example, synaptic inputs may affect much more strongly the timing of next Purkinje cell spike if they occur long after the previous Purkinje cell spike (Phoka *et al.* 2010; Couto *et al.* 2015). Therefore, the impact of a synaptic input may critically depend on the firing history of the postsynaptic cell. This may have an important impact on the computations performed in the network. We therefore set out to examine this feature *in vivo*.

In vivo, the ISI distribution has a long positive tail, precluding the definition of a proper 'rhythm' of the cells (required to define a phase). Instead, we examined a closely related quantity, the DSC, which simply measures how the discharge of the interneuron delays the discharge of the following Purkinje cell spike as a function of the interval between the interneuron spike and the previous Purkinje cell spike. Specifically, we examined the deviation from the expected latency to the next Purkinje cell spike after an interneuron spike (t_{forward}), as a function of the time elapsed between the previous Purkinje cell spike and the interneuron spike (t_{back}) (Fig. 5*A*–*D*). The expected latency to the next Purkinje spike is obtained from the Purkinje ISI distribution (see Methods). The average deviation from the expected ISI induced by interneuron spikes (Fig. 5*B*, red) appeared to be independent of the delay subsequent to the last Purkinje cell spike, as indicated by the slope of the linear fit (Fig. 5*B*, green), which was ∼0 (Fig. 5*E*). This slope was furthermore independent of the firing rate of the Purkinje cell (Fig. 5*F* and *G*, triangles).

To further investigate this phenomenon, we performed whole cell voltage-clamp recordings of Purkinje cells in sagittal slices of the cerebellar vermis from adult rats, and stimulated visually-identified basket cells in the loose cell attached configuration. The DSC of such recording was not flat (Fig. 5*C*) and generally had a positive slope (Fig. 5*E* and *G*, circles). Interneuron spikes occurring late after a Purkinje cell spike (and thus presumably just before the next Purkinje cell spike) are therefore more effective at inhibiting the cell.

During slice preparation, all the afferent fibres to the cerebellar cortex are cut. The basal level of activity is therefore reduced and the background synaptic activity is extremely low, as can be seen by the low coefficient of variation of the Purkinje cell ISIs compared to *in vivo* recordings (*in vitro*: 0.12 ± 0.06, $n = 19$, *in vivo*: 0.81 ± 0.39, $n = 27$, $P < 1 \times 10^{-4}$). To increase this background activity, we applied 100 μM furosemide, which blocks α6-containing GABA receptors found specifically on cerebellar granule cells (Korpi *et al.* 1995), and thus increases the excitability of the input layer of the cortex (Hamann *et al.* 2002). Furosemide application could reproduce a level of variation of Purkinje cell ISI similar to that observed *in vivo* (0.61 ± 0.34, $n = 5$, which is not significantly different from *in vivo*, $P = 0.17$, which is significantly different from *in vitro* without furosemide $P < 1 \times 10^{-4}$). This was, however, only possible for relatively low Purkinje cell firing rates. DSCs measured in the presence of furosemide appeared flat (Fig. 5*D*), with a smaller slope than without furosemide (Fig. 5*E*). Dense synaptic inputs producing an irregular discharge (high coefficient of variation of the ISIs) thus appear to induce a flattening of the DSC of Purkinje cells.

We examined whether the irregularity of the discharge would indeed be sufficient to explain the flat DSC. For this purpose, we built a simple two-compartment model Purkinje cell (see Methods), where the irregular discharge was produced by stochastic inputs. We found that the slope of the DSC was strongly influenced by the degree of discharge irregularity (with little impact of the firing rate) (Fig. 5*H*). In particular, flat DSCs could be observed at any firing rate, provided that the input noise produced sufficient variability (reflected in a high coefficient of variation of the ISIs).

The underlying cause of the flat DSC is directly linked to the dynamics of membrane potential in irregular-discharging neurons, as described previously within the framework of a simple single-compartment model (Ostojic, 2011). For a fixed discharge rate, the firing mode of the neuron progressively changes as the fluctuating part of its inputs increases. In the absence of fluctuating inputs, the neuron fires perfectly periodically as a result of a tonic depolarizing input (Fig. 6*D*),

and the phase of any additional input strongly affects the timing of the next action potential (Fig. 6*G*). This corresponds to the cases observed *in vitro* under the low noise condition (Figs 5*C* and 6*A*). As the magnitude of the input fluctuations is increased, the same firing rate is obtained with a smaller mean depolarizing part and the firing becomes more irregular. Eventually, the mean input becomes insufficient to drive the neuron above threshold. The firing of the neuron becomes driven by the fluctuations that stochastically hyperpolarize or depolarize the membrane potential and deflect it from the mean subthreshold depolarization produced by the

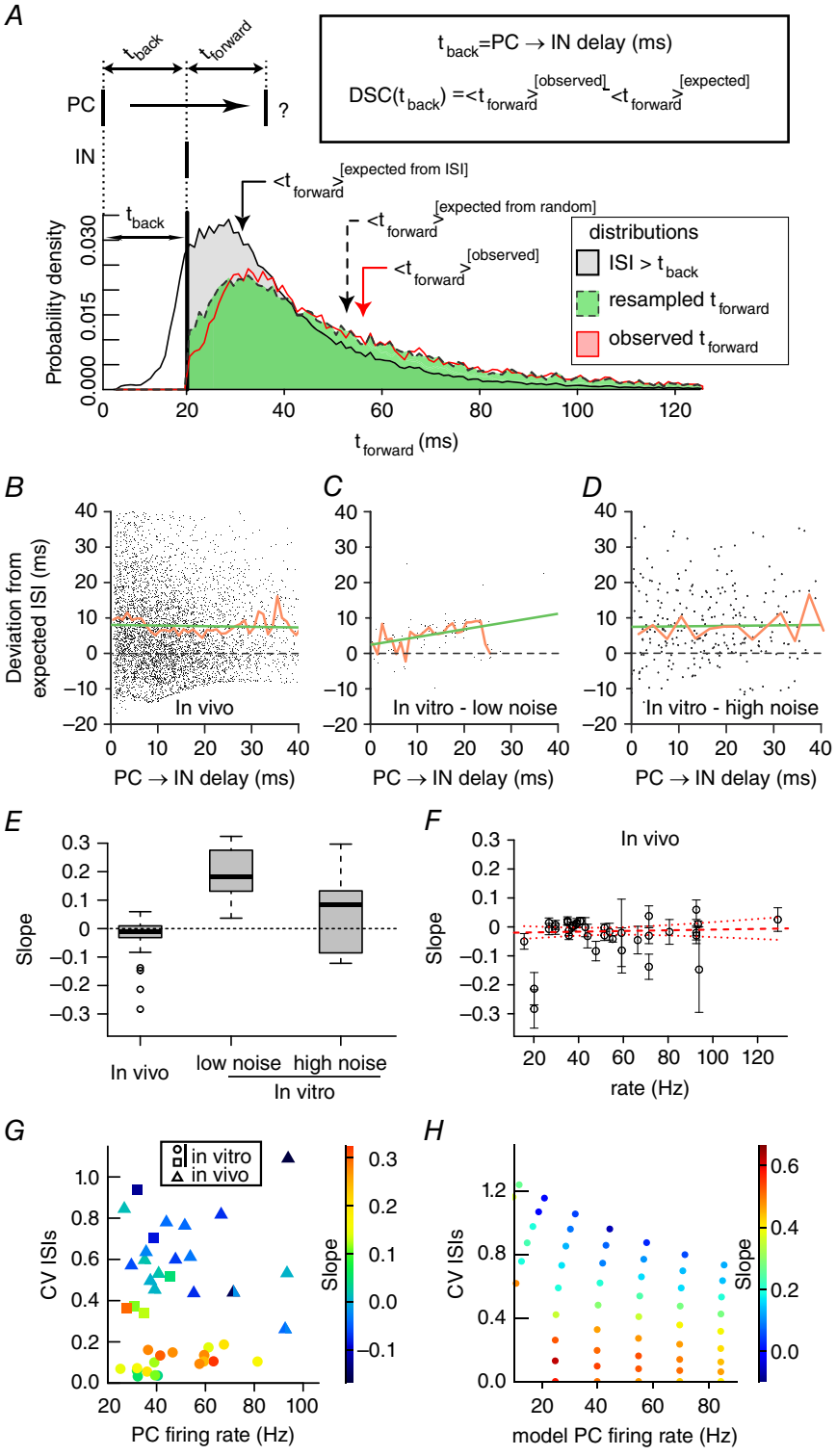

Figure 5. The inhibition-induced delay is independent of the Purkinje cell firing cycle in irregular neurons
A, principle of the DSC computation (detailed in the Method section): the DSC detects how the average delay $t_{forward}$ from an interneuron (IN) spike to the next Purkinje cell (PC) spike deviates from the expected average value, as a function of the delay t_{back} between the interneuron spike and the previous PC spike; the expected value is derived either from the ISI distribution (grey), or from the distribution of the $t_{forward}$ obtained with a randomized interneuron spike train (obtained by shuffling of the interneuron ISI, green; this distribution is shifted to the right compared to the ISI distribution because randomly shuffled interneuron spikes have more chances to fall in long ISIs than in short ISIs). *B–D*, example of DSC (i.e. the deviation from expected latency, $t_{forward}$, as a function of the delay subsequent to the last Purkinje cell spike (t_{back}). Black dots are individual spikes; red curve is the average using 1 ms bins; and green shows the best linear fit. *B*, *in vivo*, the latency does not depend on the delay subsequent to the last Purkinje cell spike. *C*, *in vitro*, under the low noise condition, ISIs occurring after interneuron spikes late in the Purkinje cell firing cycle (longer t_{back} and shorter expected $t_{forward}$) deviate more from the expected value than those occurring early. *D*, increasing noise level *in vitro* lowers the DSC slopes, which become closer to that observed *in vivo*. *E*, population boxplot of the slope of linear fit (green curves in *B–D*) for all tested cells. *F*, values of the DSC slope (with confidence interval) for pairs recorded *in vivo*, as a function of the PC firing rate. Red lines: linear fit and confidence interval on the slope value (not significantly different from 0; $P = 0.65$). *G*, slope of linear fit across all recording conditions. Triangles, *in vivo*; squares: *in vitro* high noise; circles: *in vitro* low noise. *H*, a simple model (see Methods) qualitatively reproduces the dependence of the DSC slope on the coefficient of variation of the ISIs.

input mean. In this regime, as the time after the previous action potential increases, the membrane potential progressively forgets when it last crossed the threshold, and the dynamics eventually become independent of the time subsequent to the last spike (Ostojic, 2011). This 'loss of memory' (at a fixed discharge rate) leads to an exponential tail in the distribution of interspike intervals (Fig. 6*E* and *F*), as observed *in vivo* (Fig. 6*B* and *C*), and implies that any additional input has an effect that is independent of its timing subsequent to the last action potential. The DSC therefore becomes flat at input times larger than the memory time of the system (Fig. 6*H* and *I*). The memory time moreover decreases as the magnitude of the fluctuations is increased. Consequently, the DSC becomes progressively flatter as the irregularity of the firing increases.

Lack of evidence for the involvement of interneurons in fast oscillations organizing the Purkinje cell population

Finally, as noted above, interneurons did not exhibit, in their cross-correlograms, the fast 200 Hz ripples found in the Purkinje cells and associated with fast cerebellar oscillations (de Solages *et al.* 2008). To further investigate whether interneurons participate in the 200 Hz oscillations, we calculated the average of the unfiltered local field potential (LFP) around spike times (spike-triggered average, Fig. 7*A* and *B*). Spike-triggered averages of the LFP for Purkinje cells (Fig. 7*A* and *B*, red) revealed oscillations in the form of a ripple around the spike, indicative of phase-locking of the spike to a local oscillation. The power spectrum of the spike-triggered

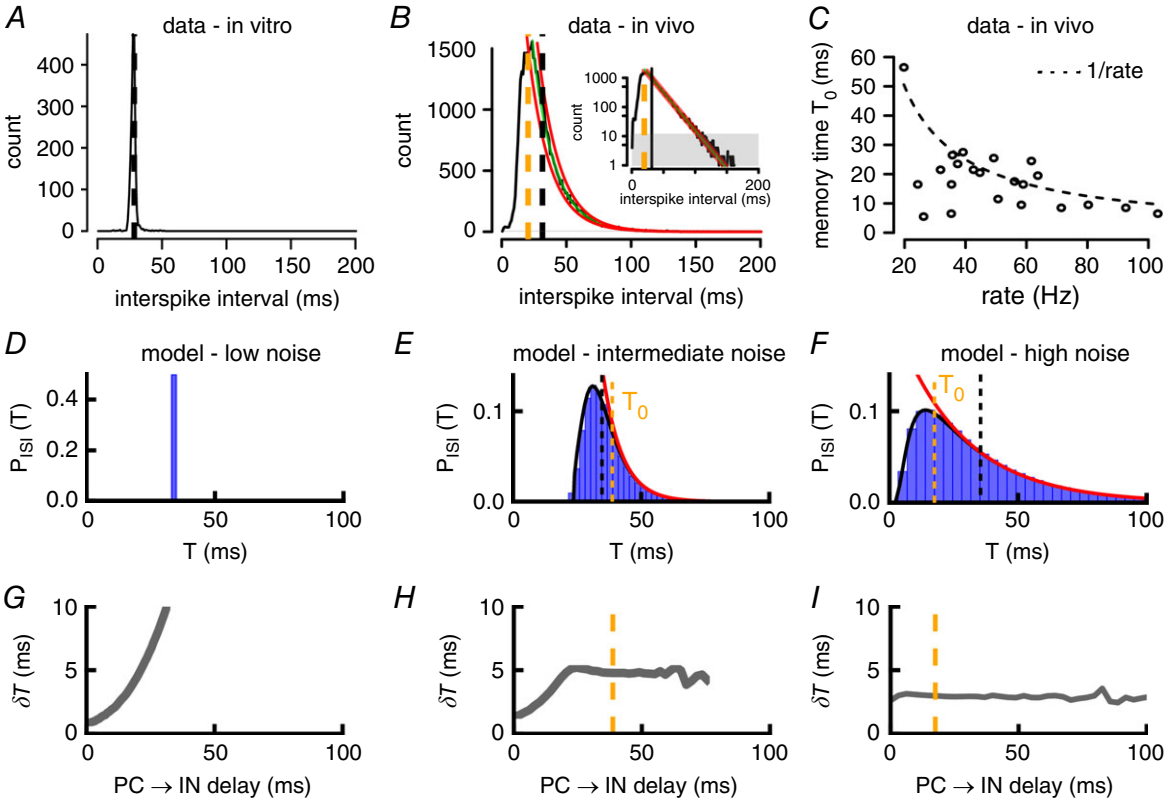

Figure 6. The forgetful neuron: long-tailed ISI distributions are associated with flat DSC
Illustration of the relationship between firing irregularity and flat DSC (i.e. independence of the impact of a synaptic input to the recent firing history of the postsynaptic cell) in a single-compartment model of Purkinje cell. *A* and *B*, example of ISI distribution of PC recorded *in vitro* (*A*) and *in vivo* (*B*). The mean ISI is indicated by a black dashed line and the memory time (*B*) is indicated by an orange dashed line. An exponential fit (see Methods) of the tail of the ISI distribution (green, fit; red, confidence interval) has been overlaid on the histogram. The greyed area indicates the part of the histogram with less than 10 counts per bin, which was not taken into account for the fit. *B*, inset: ISI distribution and fit in logarithmic scale. *C*, memory time constant for Purkinje cell recordings *in vivo* is generally lower than the average ISI (1/rate), $P = 0.03$. *D*–*F*, distribution of interspike intervals as their CV is increased (CV = 0, 0.22 and 0.75, respectively in *D*, *E* and *F*), at the same time as the mean discharge rate is kept constant (30 Hz, dashed black line). This is achieved by increasing the variance of the fluctuating input at the same time as lowering its mean. The memory time T_0 (orange line) is defined as the time at which the tail of the distribution becomes exponential (Ostojic, 2011). *G*–*I*, DSCs corresponding to (*D*) to (*F*).

average exhibits a peak at ∼200 Hz (Fig. 7*C*, blue), at the same frequency as the peak of the LFP power spectrum computed for the whole recording (Fig. 7*D*, blue, slope = 1.03, $r_2 = 0.58$, $P < 1 \times 10^{-5}$). By contrast, no oscillation was detected in the molecular layer interneuron spike-triggered averages (Fig. 7*A* and *B*, red). Accordingly, their power spectra were relatively flat, with a broad peak at much slower frequency (∼50 Hz) (Fig. 7*C*; note, however, in the panel inset showing all interneuron spectra, that a small peak at ∼170 Hz is seen for one interneuron, in green), which was independent of the LFP power spectrum peak (Fig. 7*D*, red, $P = 0.9$). Therefore, the interneurons recorded in the present study do not appear to participate in the high-frequency oscillations organizing the Purkinje cell activity.

Discussion

Simultaneous recording of molecular layer interneurons and Purkinje cells

In the present study, we simultaneously recorded two types of units. Purkinje cells can be formally identified by the presence of complex spikes. However, even in the absence of identified complex spikes, the relatively high firing rate and shape of the cross-correlogram permit the unambiguous classification of Purkinje cells. Very fast (∼200 Hz) oscillations are systematically visible both in cross-correlograms and in the LFP averaged around Purkinje cell spikes (de Solages *et al.* 2008).

The other type of units recorded never exhibited complex spikes, had a slower firing rate than Purkinje cells, had a wider distribution of interspike intervals, and did not show a trace of fast oscillations in cross-correlograms and spike-triggered average of the LFP. They did not present any of the distinctive firing properties of Golgi cells (Vos *et al.* 1999) but presented multiple characteristics of molecular layer interneurons. First, they appeared to inhibit Purkinje cells monosynaptically, a feature also reported for the Lugaro cell (Dean *et al.* 2003), a much less frequent and less characterized cell type. The physiology of Lugaro cells is still relatively unknown. They are, however, less numerous than basket cells and do not appear to mediate a strong direct effect on Purkinje cells because their activation by serotonin decreases inhibitory synaptic activity in Purkinje cells (Dieudonné and Dumoulin, 2000). They therefore probably do not represent a significant percentage of our sample. Second, the discharge statistics of our slow units match with values found in identified molecular layer interneurons and discriminate these cell types from other units in the cerebellar cortex (Ruigrok *et al.* 2011; Van Dijck *et al.* 2013). Third, in our recordings, pairs of these slow units displayed cross-correlograms with a ∼3 ms synchrony, which is similar to those reported *in vitro* for molecular layer interneurons (Mann-Metzer & Yarom, 1999). Finally, because these cells were recorded together with Purkinje cells, they are located close to the Purkinje cell layer and are thus probably basket cells.

Interneurons mediate feed-forward inhibition

In vivo recordings are performed under conditions of intense background synaptic activity resulting in irregular firing discharge (high coefficient of variation of the ISIs) and offering the opportunity to study the functional connectivity in the network. The cross-correlograms between interneurons and Purkinje cells indicate that the former preferentially discharge in the milliseconds following a Purkinje cell spike. We confirmed that (1) the increased Purkinje discharge before the interneuron was not the result of a disinhibition of Purkinje cells; (2) the inhibition was still observed if we took into account the increased Purkinje cell spike count before the

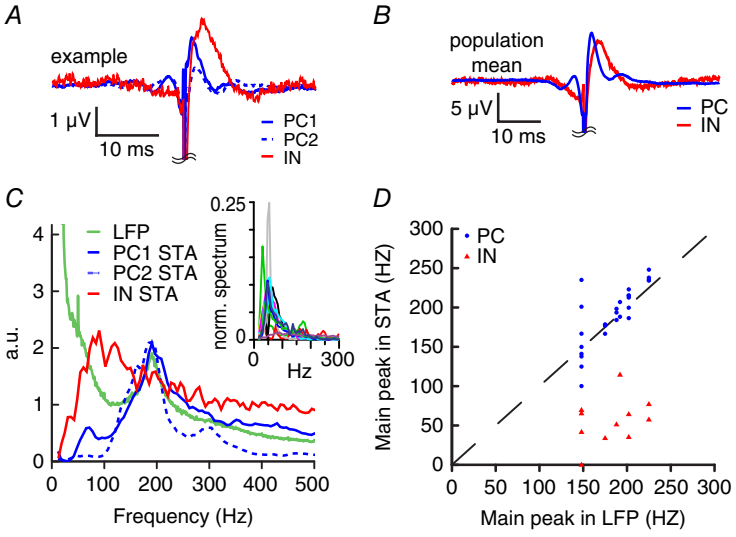

Figure 7. Interneurons are not involved in fast oscillations of Purkinje cells
A, superimposed spike-triggered average (STA) of one interneuron and two Purkinje cells from the same 30 min recording. A ∼200 Hz wave is visible in the STA of Purkinje cells (blue) but not in that of the interneuron (red). *B*, same as *A* for the cell population (26 Purkinje cells and 11 interneurons). *C*, superimposed power spectra of values (same cells as in *A*) and of the local field potential (LFP, green). The high-frequency component is present in the LFP and in the STA of the Purkinje cells (blue) but not in that of the interneuron (red). Inset: power spectrum of the STA of all the interneurons; there is no peak at high frequency (except maybe a small peak for the cell plotted in green).
D, peak frequency in the spectra of STA values is correlated with the peak frequency in the spectra of the LFP for Purkinje cells (red) but not interneurons (blue).

interneuron; (3) the pattern of the correlogram was reproduced by a simple model of feed-forward inhibition; and (4) it was observed in intracellular recordings *in vitro* under conditions of increased background activity. We therefore suggest that this pattern of firing results from feed-forward inhibition.

The timing of the Purkinje cell excitation/inhibition sequence around the interneuron spikes is close to the 5–10 ms delay recorded *in vitro* between the glutamatergic current and the disynaptic inhibitory current in the Purkinje cell in response to granule stimulation (at room temperature) (Barbour, 1993). Such a pattern of consecutive excitation and inhibition in Purkinje cell firing following the stimulation of beams of parallel fibres has been previously described *in vivo* (Andersen *et al.* 1964; Eccles *et al.* 1967) and *in vitro* (Barbour, 1993; Brunel *et al.* 2004; Mittmann *et al.* 2005). It is a predominant feature of activation in response to extracellular stimulation in the granule cell layer or in the molecular layer *in vitro*. It can also be seen after single granule cell stimulation (Barbour, 1993) and is classically interpreted as the signature of feed-forward inhibition. Feed-forward inhibition also appeared to be largely present in a study of the functional impact on Purkinje cell discharge of focal stimulations in the granule layer, as long as interneurons and Purkinje cells probably had overlapping dendritic trees (Dizon & Khodakhah, 2011).

However, the relevance of a feed-forward inhibitory circuit has been questioned by experiments mapping the cutaneous receptive fields in unanaesthetized decerebrated animals. The cutaneous stimulation that evoked Purkinje cell or activity without complex spikes allowed the identification of 'parallel fibre' somatosensory receptive fields. Parallel fibre receptive fields for Purkinje cells were always disjoint from the receptive fields of interneurons recorded nearby (Ekerot & Jörntell, 2001; Jörntell & Ekerot, 2002; Jörntell *et al.* 2010), suggesting that separated parallel fibres excite the adjacent Purkinje cells and interneurons.

Under the conditions of the present study, both independent and shared excitation onto Purkinje cells and interneurons were required to reproduce, in a model of the interneuron–Purkinje cell network, the features of the cross-correlograms obtained with our recordings. This indicates that a subset of the excitatory inputs in the network is shared by interneurons and Purkinje cells. The amplitude and time constant of the post-synaptic inhibitory current at the interneuron → Purkinje cell synapses *in vivo* used in the model (peak conductance: $g_{syn} = 0.4$ nS, decay time $\tau_d = 3$ ms) are in accordance with *in vitro* measurements performed unnder physiological conditions (Houston *et al.* 2009).

Patterns of feed-forward inhibition, with increased and decreased firing of Purkinje cells respectively before and after the interneuron spikes, appear almost ubiquitous under our conditions. Indeed, the strength of the inhibition that an interneuron mediates is strongly correlated with the level of excitation it shares with its target (Fig. 3*A* and *D*).

Interestingly, bursts of intense parallel fibre excitatory inputs triggering trains of Purkinje cells spikes have also been shown to trigger long (15–150 ms) pauses, which increased in duration with the intensity of the incoming excitation and did not involve inhibitory inputs, and which might signal learned input patterns (Steuber *et al.* 2007); our results suggest that feed-forward inhibition might participate in similar encoding at shorter time-scales (<10 ms). Feed-forward inhibition does not appear to be prominent for sensory inputs in the paravermal area (Ekerot & Jörntell, 2001; see above, although the recorded interneurons in these studies may have been mostly stellate cells, whereas the present study, which is using spontaneous instead of evoked activity, probably focused on basked cells), although it has been observed in hemispheres for facial stimulations (Santamaria *et al.* 2007; Chu *et al.* 2012). Further studies will be needed to determine whether, for example, feed-forward inhibition is preferentially present in response to non-sensory inputs such as cortico-cerebellar inputs, which are cut in decerebrated preparations (Ekerot and Jörntell, 2001), or whether the predominance of these patterns of connectivity is unevenly distributed in the cerebellum.

Dynamics of inhibition *in vivo*

Inhibition of Purkinje cells by molecular layer interneurons has been extensively studied *in vitro* in young animals, where strong inputs can affect Purkinje cell firing (Häusser & Clark, 1997). These inhibitory connections are developmentally regulated and much smaller in the adult (Pouzat & Hestrin, 1997). The currents that we recorded in slices were indeed small and in agreement with the recordings of Pouzat & Hestrin (1997) (taking into account the reduced driving force in our conditions, with a low chloride internal solution). This reduced amplitude in adult animals might explain why the only study that recorded interneuron–Purkinje cell pairs *in vivo* (Bengtsson *et al.* 2013) reported little effect of molecular layer interneurons on Purkinje cells. In the present study, we show that inhibition induced by putative basket cells is indeed very brief but quite strong. Bengtsson *et al.* (2013) used loose-patch dual extracellular recordings, and targeted neurons less than 10 μm apart, which could explain the discrepancy with our observations. With our tetrode recordings (with contact distances ~30 μm), interneurons are probably in a ~50 μm radius around Purkinje cells. Basket cells might therefore have smaller connections with Purkinje cells directly apposed to their soma than with those positioned a few tens of microns laterally, as their axonal morphology suggests (Bishop, 1993).

The onset of inhibition cannot be resolved in our cross-correlograms because simultaneous spikes are difficult to isolate and have therefore been excluded. It nonetheless appears to be rapid, as close to the extracellular interneuron spike as can be resolved by our technique (Fig. 2*G–I*). This absence of delay might be a result of the action of coupled interneurons, some of which, on average, would fire before the one recorded. It could also be explained by the extremely fast ephaptic inhibition of Purkinje cells through basket cell pinceaux (Blot & Barbour, 2014).

The short duration of inhibition of Purkinje cell discharge fits with previous reports of the fast somatic inhibitory currents (decay time close to 3 ms) in Purkinje cells (de Solages *et al.* 2008; Houston *et al.* 2009). This suggests that the somatic synaptic potentials have a decay close to the decay of synaptic currents. This requires a fast somatic membrane constant, which probably results from the low-resistance coupling of the somatic compartment with the large dendritic compartment in the Purkinje cells (de Solages *et al.* 2008; Ostojic *et al.* 2015).

The forgetful neuron

We found that, *in vivo*, the average delay in Purkinje spike times induced by the interneurons input is independent of the timing of the Purkinje spike that preceded the synaptic input. This may be interpreted as a sign that Purkinje cells act as perfect integrator by exactly compensating its leak current via an unresolved biophysical process (Phoka *et al.* 2010; Couto *et al.* 2015). Our *in vitro* and modelling experiments support an alternate view, where, because of the intense incoming synaptic activity, the dynamics of Purkinje cell membrane potential is weakly dependent on the previous synaptic inputs and firing history (Ostojic, 2011) and is thus deterministic only on short time scales.

Under all the three conditions (*in vivo*, *in vitro* low noise and *in vitro* high noise), the slope of the DSC appeared to be only weakly dependent of the cell firing rate in our experiments (Fig. 5*E–G*). This appears contradictory to the observation of Phoka *et al.* (2010), where Purkinje cell with a low firing rate tend to have a flatter phase response curve, even for a low coefficient of variation of the ISI (Couto *et al.* 2015). The cause of this discrepancy is unclear, although it might be explained by differences in the preparation (we are studying Purkinje cells from adult rats, in contrast to the immature rats used in these studies) and/or recording conditions. Indeed, a subset of the Purkinje cell that we recorded *in vitro* exhibited a very low coefficient of variation of ISI, and only a mild slope of their DSC (cluster of points in the bottom left in Fig. 5*G*); therefore, the cases described by Phoka *et al.* (2010) and Couto *et al.* (2015) could correspond to cases of highly regular Purkinje cell discharge that are less frequent *in vitro* in adult Purkinje cells and are not observed *in vivo*.

The firing of Purkinje cells have also been proposed to exhibit some degree of temporal structure at longer time scales than those employed in the present study, with alternating periods of short, regular, ISIs and long irregular ISIs ('pauses'; Shin *et al.* 2007). The mechanisms promoting these two regimes are not yet fully resolved, although our DSC analysis suggests that the impact of the interneurone on PC firing is similar in both conditions.

In vivo, because of the strong level of synaptic activity and possibly also the complex spike-dependent processes (Cerminara & Rawson, 2004), Purkinje cell discharge is irregular and the underlying membrane potential dynamics may thus be characterized as having a short memory time compared to the extent of the ISI distribution. The function of inhibition by interneurons might therefore be to reduce the probability of firing during a short time, corresponding to one 200 Hz oscillation cycle. This convergence of time scales for synaptic integration and the organization of population activity might indicate that the fundamental operation clock of the cerebellum, which has been described as specialized in timing with millisecond precision (Ivry & Spencer, 2004; Zatorre *et al.* 2007; D'Angelo & de Zeeuw, 2009), is ∼5–10 ms.

References

Abramoff MD, Magalhães PJ & Ram SJ (2004). Image processing with ImageJ. *Biophotonics Int* **11**, 36–42.

Andersen P, Eccles J & Voorhoeve P (1964). Postsynaptic inhibition of cerebellar Purkinje cells. *J Neurophysiol* **27**, 1138–1153.

Ascoli GA, Alonso-Nanclares L, Anderson SA, Barrionuevo G, Benavides-Piccione R, Burkhalter A, Buzsáki G, Cauli B, DeFelipe J, *et al.* (2008). Petilla terminology: nomenclature of features of GABAergic interneurons of the cerebral cortex. *Nat Rev Neurosci* **9**, 557–568.

Badel L, Lefort S, Brette R, Petersen CCH, Gerstner W & Richardson MJE (2008). Dynamic I-V curves are reliable predictors of naturalistic pyramidal-neuron voltage traces. *J Neurophysiol* **99**, 656–666.

Barbour B (1993). Synaptic currents evoked in Purkinje cells by stimulating individual granule cells. *Neuron* **11**, 759–769.

Bengtsson F, Geborek P & Jörntell H (2013). Cross-correlations between pairs of neurons in cerebellar cortex in vivo. *Neural Netw* **47**, 88–94.

Bishop GA (1993). An analysis of HRP-filled basket cell axons in the cat's cerebellum. *Anat Embryol* **188**, 287–297.

Blot A & Barbour B (2014). Ultra-rapid axon-axon ephaptic inhibition of cerebellar Purkinje cells by the pinceau. *Nat Neurosci* **17**, 289–295.

Brunel N, Hakim V, Isope P, Nadal J-P & Barbour B (2004). Optimal information storage and the distribution of synaptic weights: perceptron versus Purkinje cell. *Neuron*, **43**, 745–757.

Cerminara N & Rawson J (2004). Evidence that climbing fibers control an intrinsic spike generator in cerebellar Purkinje cells. *J Neurosci* **24**, 4510–4517.

Chu C, Bing Y, Liu H & Qiu D (2012). Roles of molecular layer interneurons in sensory information processing in mouse cerebellar cortex Crus II in vivo. *PloS ONE* **7**, e37031.

Cohen D & Yarom Y (2000). Cerebellar on-beam and lateral inhibition: two functionally distinct circuits. *J Neurophysiol* **83**, 1932–1940.

Couto J, Linaro D, De Schutter E & Giugliano M (2015). On the firing rate dependency of the phase response curve of rat purkinje neurons in vitro. *PLoS Comput Biol* **11**, e1004112.

Csicsvari J, Hirase H, Czurko A, Mamiya A & Buzsáki G (1999). Fast network oscillations in the hippocampal CA1 region of the behaving rat. *J Neurosci* **19**, RC20.

de Solages C, Szapiro G, Brunel N, Hakim V, Isope P, Buisseret P, Rousseau C, Barbour B & Léna C (2008). High-frequency organization and synchrony of activity in the purkinje cell layer of the cerebellum. *Neuron* **58**, 775–788.

De Zeeuw CI & Berrebi AS (1995). Postsynaptic targets of Purkinje cell terminals in the cerebellar and vestibular nuclei of the rat. *Eur J Neurosci* **7**, 2322–2333.

Dean I, Robertson SJ & Edwards FA (2003). Serotonin drives a novel GABAergic synaptic current recorded in rat cerebellar purkinje cells: a Lugaro cell to Purkinje cell synapse. *J Neurosci* **23**, 4457–4469.

DeFelipe J, López-Cruz PL, Benavides-Piccione R, Bielza C, Larrañaga P, Anderson S, Burkhalter A, Cauli B, Fairén A, *et al.* (2013). New insights into the classification and nomenclature of cortical GABAergic interneurons. *Nat Rev Neurosci* **14**, 202–216.

Delescluse M & Pouzat C (2006). Efficient spike-sorting of multi-state neurons using inter-spike intervals information. *J Neurosci Methods* **150**, 16–29.

Dieudonné S & Dumoulin A (2000). Serotonin-driven long-range inhibitory connections in the cerebellar cortex. *J Neurosci* **20**, 1837–1848.

Dizon MJ & Khodakhah K (2011). The role of interneurons in shaping Purkinje cell responses in the cerebellar cortex. *J Neurosci* **31**, 10463–10473.

D'Angelo E & De Zeeuw CI (2009). Timing and plasticity in the cerebellum: focus on the granular layer. *Trends Neurosci* **32**, 30–40.

Eccles JC, Ito M & Szentágothai J (1967). *The Cerebellum as a Neuronal Machine*. Springer-Verlag, Berlin.

Ekerot C-F & Jörntell H (2001). Parallel fibre receptive fields of Purkinje cells and interneurons are climbing fibre-specific. *European Journal of Neuroscience*, **13**, 1303–1310.

Ermentrout B & Terman DH (2010). *Mathematical Foundations of Neuroscience*. Interdisciplinary Applied Mathematics. Springer, New York, NY.

Fourcaud-Trocmé N, Hansel D, van Vreeswijk C & Brunel N (2003). How spike generation mechanisms determine the neuronal response to fluctuating inputs. *J Neurosci* **23**, 11628–11640.

Gao H, Solages CD & Lena C (2012). Tetrode recordings in the cerebellar cortex. *J Physiol Paris* **106**, 128–136.

Hamann M, Rossi D & Attwell D (2002). Tonic and spillover inhibition of granule cells control information flow through cerebellar cortex. *Neuron* **33**, 625–633.

Heiney S, Kim J, Augustine G & Medina J (2014). Precise control of movement kinematics by optogenetic inhibition of Purkinje cell activity. *J Neurosci* **34**, 2321–2330.

Holt G, Softky W, Koch C & Douglas R (1996). Comparison of discharge variability in vitro and in vivo in cat visual cortex neurons. *J Neurophysiol* **75**, 1806–1814.

Houston CM, Bright DP, Sivilotti LG, Beato M & Smart TG (2009). Intracellular chloride ions regulate the time course of GABA-mediated inhibitory synaptic transmission. *J Neurosci* **29**, 10416–10423.

Häusser M & Clark BA (1997). Tonic synaptic inhibition modulates neuronal output pattern and spatiotemporal synaptic integration. *Neuron* **19**, 665–678.

Isope P & Barbour B (2002). Properties of unitary granule cell→Purkinje cell synapses in adult rat cerebellar slices. *J Neurosci* **22**, 9668–9678.

Isope P, Dieudonné S & Barbour B (2002). Temporal organization of activity in the cerebellar cortex: a manifesto for synchrony. *Ann NY Acad Sci* **978**, 164–174.

Ivry RB & Spencer RM (2004). The neural representation of time. *Curr Opin Neurobiol* **14**, 225–232.

Johnson D & Kiang N (1976). Analysis of discharges recorded simultaneously from pairs of auditory nerve fibers. *Biophys J* **16**, 719–734.

Jörntell H, Bengtsson F, Schonewille M & De Zeeuw CI (2010). Cerebellar molecular layer interneurons – computational properties and roles in learning. *Trends Neurosci* **33**, 524–532.

Jörntell H & Ekerot C-F (2002). Reciprocal bidirectional plasticity of parallel fiber receptive fields in cerebellar Purkinje cells and their afferent interneurons. *Neuron* **34**, 797–806.

Jörntell H & Ekerot C-F (2003). Receptive field plasticity profoundly alters the cutaneous parallel fiber synaptic input to cerebellar interneurons in vivo. *J Neurosci* **23**, 9620–9631.

Kim J, Lee S, Tsuda S, Zhang X, Asrican B, Gloss B, Feng G & Augustine GJ (2014). Optogenetic mapping of cerebellar inhibitory circuitry reveals spatially biased coordination of interneurons via electrical synapses. *Cell Rep* **7**, 1601–1613.

Klausberger T & Somogyi P (2008). Neuronal diversity and temporal dynamics: the unity of hippocampal circuit operations. *Science* **321**, 53–57.

Ko H, Hofer SB, Pichler B, Buchanan KA, Sjöström PJ & Mrsic-Flogel TD (2011). Functional specificity of local synaptic connections in neocortical networks. *Nature* **473**, 87–91.

Korpi ER, Kuner T, Seeburg PH & Lüddens H (1995). Selective antagonist for the cerebellar granule cell-specific gamma-aminobutyric acid type A receptor. *Mol Pharmacol* **47**, 283–289.

Lamsa K, Heeroma JH & Kullmann DM (2005). Hebbian LTP in feed-forward inhibitory interneurons and the temporal fidelity of input discrimination. *Nat Neurosci* **8**, 916–924.

Mann-Metzer P & Yarom Y (1999). Electrotonic coupling interacts with intrinsic properties to generate synchronized activity in cerebellar networks of inhibitory interneurons. *J Neurosci* **19**, 3298–3306.
Mittmann W, Koch U & Häusser M (2005). Feed-forward inhibition shapes the spike output of cerebellar Purkinje cells. *J Physiol* **563**, 369–378.
Orduz D & Llano I (2007). Recurrent axon collaterals underlie facilitating synapses between cerebellar Purkinje cells. *Proc Natl Acad Sci USA* **104**, 17831–17836.
Ostojic S (2011). Interspike interval distributions of spiking neurons driven by fluctuating inputs. *J Neurophysiol* **106**, 361–373.
Ostojic S, Brunel N & Hakim V (2009). How connectivity, background activity, and synaptic properties shape the cross-correlation between spike trains. *J Neurosci* **29**, 10234–10253.
Ostojic S, Szapiro G, Schwartz E, Barbour B, Brunel N & Hakim V (2015). Neuronal morphology generates high-frequency firing resonance. *J Neurosci* **35**, 7056–7068.
Palay S & Chan-Palay V (1974). *Cerebellar Cortex: Cytology and Organization.* Springer, New York, NY.
Park S-M, Tara E & Khodakhah K (2012). Efficient generation of reciprocal signals by inhibition. *J Neurophysiol* **107**, 2453–2462.
Person AL & Raman IM (2011). Purkinje neuron synchrony elicits time-locked spiking in the cerebellar nuclei. *Nature* **481**, 502–505.
Person AL & Raman IM (2012). Synchrony and neural coding in cerebellar circuits. *Front Neural Circuits* **6**: 97.
Phoka E, Cuntz H, Roth A & Häusser M (2010). A new approach for determining phase response curves reveals that purkinje cells can act as perfect integrators. *PLoS Comput Biol* **6**, e1000768.
Pouille F & Scanziani M (2001). Enforcement of temporal fidelity in pyramidal cells by somatic feed-forward inhibition. *Science* **293**, 1159–1163.
Pouzat C & Chaffiol A (2009). Automatic spike train analysis and report generation. An implementation with R, R2HTML and STAR. *J Neurosci Methods* **181**, 119–144.
Pouzat C & Hestrin S (1997). Developmental regulation of basket/stellate cell→Purkinje cell synapses in the cerebellum. *J Neurosci* **17**, 9104–9112.
Rieubland S, Davie JT, Roth A & Häusser M (2008). The dynamic current-voltage relation of cerebellar Purkinje cells. *Soc Neuro Abs.* 44.16.
Rieubland S, Roth A & Häusser M (2014). Structured connectivity in cerebellar inhibitory networks. *Neuron* **81**, 913–929.
Rothman JS, Cathala L, Steuber V & Silver RA (2009). Synaptic depression enables neuronal gain control. *Nature* **457**, 1015–1018.
Rudolph M, Pospischil M, Timofeev I & Destexhe A (2007). Inhibition determines membrane potential dynamics and controls action potential generation in awake and sleeping cat cortex. *J Neurosci* **27**, 5280–5290.
Ruigrok TJH, Hensbroek RA & Simpson JI (2011). Spontaneous activity signatures of morphologically identified interneurons in the vestibulocerebellum. *J Neurosci* **31**, 712–724.
Santamaria F, Tripp PG & Bower JM (2007). Feedforward inhibition controls the spread of granule cell-induced Purkinje cell activity in the cerebellar cortex. *J Neurophysiol* **97**, 248–263.
Shin S-L, Hoebeek FE, Schonewille M, De Zeeuw CI, Aertsen A & De Schutter E (2007). Regular patterns in cerebellar Purkinje cell simple spike trains. *PLoS ONE* **2**, e485.
Siapas AG, Lubenov EV & Wilson MA (2005). Prefrontal phase locking to hippocampal theta oscillations. *Neuron* **46**, 141–151.
Sotelo C & Llinás R (1972). Specialized Membrane junctions between neurons in the vertebrate cerebellar cortex. *J Cell Biol* **53**, 271–289.
Steuber V, Mittmann W, Hoebeek F, Silver R, De Zeeuw C, Häusser M & De Schutter E (2007). Cerebellar LTD and pattern recognition by Purkinje cells. *Neuron* **54**, 121–136.
Stuurman N, Amdodaj N & Vale R (2007). Micro-Manager: open source software for light microscope imaging. *Micros Today* **15**, 42–43.
Van Dijck G, Van Hulle MM, Heiney SA, Blazquez PM, Meng H, Angelaki DE, Arenz A, Margrie TW, Mostofi A, *et al.* (2013). Probabilistic identification of cerebellar cortical neurones across species. *PLoS ONE* **8**, e57669.
Vos BP, Maex R, Volny-Luraghi A & Schutter ED (1999). Parallel fibers synchronize spontaneous activity in cerebellar Golgi cells. *J Neurosci* **19**, RC6–RC6.
Watt AJ, Cuntz H, Mori M, Nusser Z, Sjöström PJ & Häusser M (2009). Traveling waves in developing cerebellar cortex mediated by asymmetrical Purkinje cell connectivity. *Nat Neurosci* **12**, 463–473.
Wilson MA & McNaughton BL (1993). Dynamics of the hippocampal ensemble code for space. *Science* **261**, 1055–1058.
Wulff P, Schonewille M, Renzi M, Viltono L, Sassoè-Pognetto M, Badura A, Gao Z, Hoebeek FE, van Dorp S, *et al.* (2009). Synaptic inhibition of Purkinje cells mediates consolidation of vestibulo-cerebellar motor learning. *Nat Neurosci* **12**, 1042–1049.
Zatorre RJ, Chen JL & Penhune VB (2007). When the brain plays music: auditory–motor interactions in music perception and production. *Nat Rev Neurosci* **8**, 547–558.

Additional information

Competing interests

The authors declare that they have no competing interests.

Author contributions

CdS performed the *in vivo* experiments. AB and GS performed the *in vitro* experiments. SO and VH developed and interpreted the models. CL, CdS and AB analysed the data, and with SO and VH, interpreted the results and wrote the manuscript. All authors have approved the final version of the manuscript and

agree to be accountable for all aspects of the work. All persons designated as authors qualify for authorship, and all those who qualify for authorship are listed.

Funding

This work was supported by the ANR (ANR-09-MNPS-38, ANR-11-BSV4-028 01, ANR-12-BSV4-0027, ANR-08-SYSC-005, ANR-11-0001-02, ANR-10-LABX-0087). It has also received support under the program 'Investissements d'Avenir' launched by the French Government and implemented by the ANR, with the references: ANR-10-LABX-54 MEMO LIFE, ANR-10-LABX-0087 IEC, ANR-10-IDEX-0001-02 PSL* Research University.

Acknowledgements

We thank Boris Barbour, Stéphane Dieudonné and Philippe Ascher for critically reading the manuscript, as well as members of the Cerebellum Group, Neurophysiology of Brain Circuit Group and the IBENS Neuroscience Section, for helpful discussions and/or critical comments on the manuscript.